The Islamic University of Gaza

Faculty of Graduate Studies

Electrical Engineering Department

Nonlinear Composite Left/Right handed Transmission Line Media with RTD

By

Mahmoud O. Abu-marasa

Supervisor

Prof. Dr. Hala J. El-Khozondar

A Thesis Submitted in Partial Fulfillment of the Requirements for the Degree of Master in Electrical Engineering

2014

Abstract

The composite right/left-handed (CRLH) transmission line (TL) is presented as a general TL possessing both left-handed (LH) and right-handed (RH) natures. RH materials have both positive permittivity and positive permeability, and LH materials have both negative permittivity and negative permeability. In this work, we designed and analyzed a nonlinear CRLH-TL media with Resonant Tunneling Diode (RTD).

There are two goals of this work. The first goal is to design transmission line capable of filtering and amplifying high frequency signals at very widebands. In this case, we designed a compact ultra-wideband (UWB) filter capable of amplifying input signal with an additional power added to the output signal that equals 50% of the input signal. The bandwidth pass band of the filter goes from 5-10.5 GHz. This is satisfied by added RTD to CRLH-TL. The second goal is to design voltage controlled oscillator (VCO). The VCO model is constructed by combining the RTD with one cell of CRLH-TL. In this case, we designed three prototype device examples. The first one is a one cell with short circuit at the beginning of the cell between ground and patch, and 50 Ω load resistance at the end of the cell between ground and patch. The second one is similar to the first prototype but with open circuit at the beginning of the cell instated of short circuit. The third prototype consists of one cell with two 50 Ω load resistances between ground and patch at both the beginning and at the end of the cell. The RTD was biased using a variable DC voltage supply producing voltage oscillator at resistance load when the RTD biased in the negative differential resistance (NDR) region. The VCO capable of generating oscillation at frequencies in the range between 4.87- 14.9 GHz depending on the biasing DC voltage.

We used OrCAD, ADS and MATLAB softwares to analyse the proposed circuits. CRLH-TL based on modified hybrid approach, which consists of a microstrip line loaded with complementary split-rings resonators (CSRRs), series gaps, and shunt inductor, with RTD parallel to the shunt inductor is used to satisfy the goals of this work.

ملخص الرسالة

تعني هذه الرسالة بدراسة خطوط النقل غير الخطية المكونة من مواد ذات عوامل سماحية ونفاذية سالبة و أخرى ذات عوامل سماحية ونفاذية موجبة (CRLH-TL), حيث سنقوم بإضافة صمام ثنائي الرنين النفقي (RTD) إلى خطوط النقل وندرس مدى الاستفادة من إضافة هذا الصمام. هنالك هدفين رئيسيين لهذه الرسالة, الهدف الأول هو تصميم خطوط نقل قادرة على ترشيح و تكبير الإشارة الواردة إليها ذات الترددات العالية خلال طيف ترددي واسع, حيث قمنا بتصميم خط نقل قادر على تكبير إشارة الدخل بمقدار 50%, خلال الطيف الترددي 5-10.5 GHz وذلك عن طريق إضافة RTD إلى CRLH-TL, أما الهدف الثاني من للرسالة هو تصميم مذبذب إشارة متغير بتغير الجهد عليه (VCO), حيث قمنا بتصميم ثلاث نماذج مختلفة من VCO, النماذج الثلاثة صممت عن طريق إضافة RTD إلى خلية واحدة من خط النقل CRLH-TL, النموذج الاول صمم بحيث كان هنالك توصيل بين خط النقل والخط الارضي في بداية خط النقل أما في نهايته وضعت مقاومة بقيمة 50 اوم بينه وبين الخط الارضي أما النموذج الثاني فكان مثل التصميم الاول ولكن بعمل فصل بين خط النقل وبين الخط الارضي في بداية خط النقل بدل من التوصيل بينهما, أما التصميم الثالث فصمم بوضع مقاومة بقيمة 50 أوم بين خط النقل والخط الارضي في كل من بداية خط النقل ونهايته, فكانت النتيجة من هذه التصاميم الثلاثة هي توليد موجات بترددات بين 4.87 -14.9 GHz بحيث يختلف التردد باختلاف فرق الجهد الواقع على RTD. في هذه الدراسة قمنا باستخدام ثلاث برامج حاسوبية (OrCAD و ADS و MATLAB) حتى نقوم بتصميم وتحليل الدوائر المطلوبة.

Dedicated to

My father,

mother,

wife,

father in- law,

mother in- law,

kid Omar,

brothers, and

sisters.

Acknowledgements

First and foremost, all praise is due to Allah, the Almighty, who gave me the opportunity, strength, and patience to carry out this work. I would like to give my sincere gratitude to my supervisor Prof. Dr. Hala J. El-Khozondar for her continuous support, great guidance, endless help, good knowledge and perpetual inspiration she gave me. I would like to give my thanks to Dr. Rifa J. El-Khozondar and Dr. Talal F. Skaik for their valuable discussions and comments. I would like to give my thanks to the Electrical Engineering department teachers and fellow associates for their help and support during my course of study. Finally, words will not be enough to thank my family for their infinite support and patience.

Table of Contents

List of Tables

List of Figures

Abbreviations

CRLH	Composite right/left-handed.
TL	Transmission line.
LH	Left-handed.
RH	Right-handed.
RTD	Resonant Tunneling Diode**.**
NDR	Negative differential resistance.
VCO	Voltage controlled oscillator.
CSRR	Complementary split-rings resonators.
SRR	Split-rings resonator.
LH-TL	Left handed transmission line.
CMOS	Complementary Metal Oxide Semiconductor.
ADC	Analog-to-digital converters.
CRLH-TL	Composite right/left-handed Transmission line.
NLTL	Nonlinear transmission line.
UWB	Ultra-wideband
MPS	Metamaterial Phase Shifters.
VLSRR	Varactor loaded Split-rings resonator.
MTM	Metamaterial.
DPS	Double-positive media.
DNG	Double-negative.
SNG	Single-negative.
ENG	Epsilon-negative.
MNG	Mu-negative.
MMIC	Monolithic microwave integrated circuit.

1-Introduction

A TL is a device designed to guide electrical energy from one point to another. It is used, for example, to transfer the output radio frequency energy of a transmitter to an antenna. Where The TL consists of two or more parallel conductor used to connect the source to the load. The TL may be a coaxial, two-wire line, parallel-plate, planar line and microstrip line. Microstrip lines are important in integrated circuits where metallic strips or small electronic devices are deposited on dielectric substrates. These types of TL are called a conventional TL or right handed TL, A new type of TL which different from the conventional TL is called left handed TL (LH-TL) or metamaterial.

Recent advances have made possible the emergence of a new kind of materials called Metamaterials. These materials are artificial structures that can be constructed to have unconventional electromagnetic properties which are not found in nature as shown in figure 1.1. The development of this new scientific branch has given rise to numerous discoveries and technological advances based on the new properties shown by these novel materials. The electromagnetism is one of the fields in which metamaterials have found interesting applications, where these materials designed to interact with and control electromagnetic waves.

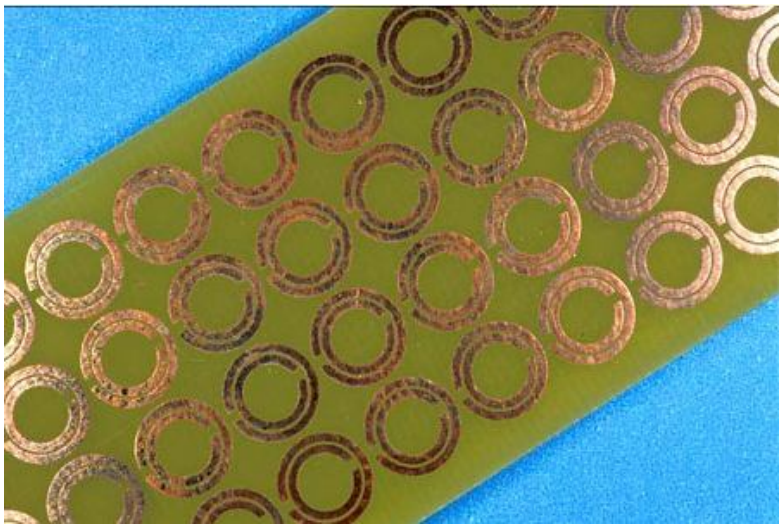

Figure 1.1: Metamaterial cells; Split rings are etched into a copper circuit board [1].

The small size and the controllability of the electrical characteristics of metamaterial TLs are the main properties that make possible their use in the synthesis of microwave devices with compact dimensions and exceptional features [2]. However, besides their small size, such devices can also offer a performance improvement for microwave devices or even new functionalities. In this thesis we concentrated on adding non-linearity component to metamaterial such as merger between metamaterial TLs and the RTD.

RTDs are currently the widest bandwidth active semiconductor devices. Which can achieve a maximum frequency of up to 2.2 THz while the Complementary Metal Oxide Semiconductor (CMOS) transistors can achieve a maximum frequency of up to 215 GHz [3]. The RTDs have more interesting referring to the high switching speed and

to the I-V characteristic that often exhibits negative differential resistance (NDR) regions. Characteristic to the current–voltage relationship of a tunneling diode is the presence of one or more NDR, which enables many unique applications. It used in wide range of application such as amplifier, pulse generators, analog-to-digital converters (ADCs) and oscillators [4].

The thesis has been divided in several sections devoted to different aspects:

- The second chapter presents a conventional electrical right handed TL and the parameters and equation of the TL.

- The third chapter presents a brief introduction about Metamaterials, and left handed materials, including their properties and constituent elements.

- The fourth chapter with a topic of composite left/right handed transmission which presents the implementation of metamaterial TLs by means of the resonant approach, which is applied in this work.

- The fifth chapter presents the RTD and their operation and voltage-current behaviors.

- The sixth chapter presents literature review and previous studies in research.

- Seventh chapter focuses on the methodology, simulation and result of our research.

- Finally, the eighth chapter includes some conclusions and possible next goals are exposed.

2- Electrical Transmission Lines

2.1 Introduction

The electrical TL is a guided structures used to direct the propagation of energy from the source to the load. The TLs are used mainly in transmitting the power at low frequencies and in communications at high frequencies. Common examples for TL in our lives are twisted wire pairs which are used in computer networks and coaxial cables which are used in TV.

The TL consists of two or more parallel conductor used to connect the source to the load. The TL may be a coaxial cable connecting TV set to TV antenna, where the TV antenna is the source and the TV set is the load. Another types of TL are the two-wire line, the parallel-plate, the planar line and the microstrip line as shown in figure 2.1. Microstrip lines are important in integrated circuits where metallic strips or small electronic devices are deposited on dielectric substrates. These types of TL are called a conventional TL or right handed TL. A new type of TL which different from the conventional TL is called left handed TL (LHTL) that will discuss later.

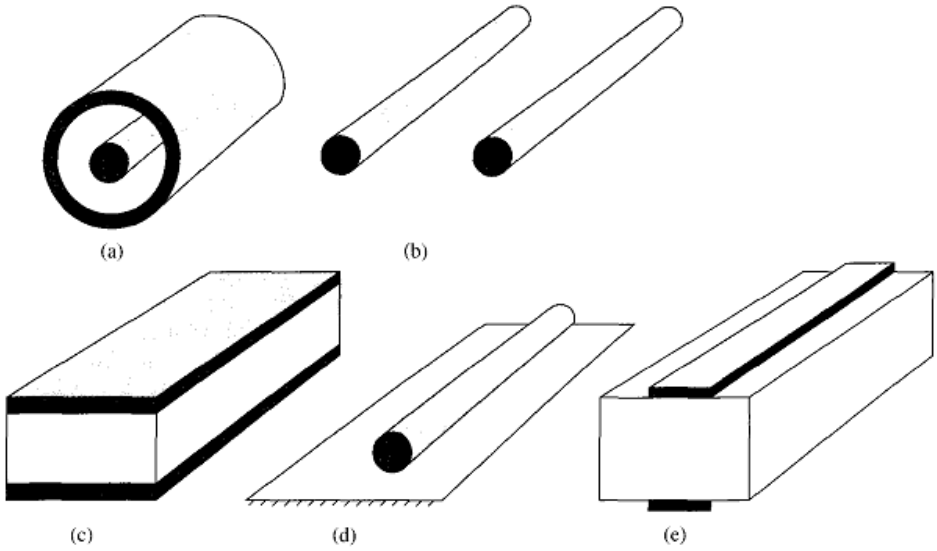

Figure 2.1: Cross section of different types of TL [5]: (a) coaxial line, (b) two-wire line, (c) planar line, (d)wire above conducting plane, and (e) microstrip line.

2.2 TL parameters

The design of a TL depends on four electrical parameters which are resistance per unit length R, inductance per unit length L, capacitance per unit length C, and conductance per unit length G. Where $G \neq 1/R$; R is AC resistance of the conductors and G is the conductance due to the dielectric that separate the conductors. The distributed parameters of a two-conductor (conventional) TL as shown in figure 2.2 where the parameters are uniformly distributed along the TL (R and L are in Series, C and G are in shunt).

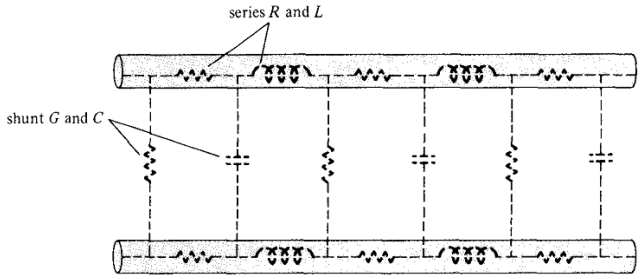

Figure 2.2: Distributed parameters of the conventional TL [5].

All types of TLs have all parameters R, L, C, and G in a special formula. However, one or more parameters can be neglected in some type of TL. Table 2.1 provides the formula of four parameters R, L, C, and G, for coaxial line, two-wire line, and planar line, where the dimensions of the lines are as shown in figure 2.3.

Parameters	**Coaxial Line**	**Two-Wire Line**	**Planar Line**
$R\,(\Omega/m)$	$\frac{1}{2\pi\delta\sigma_c}\left[\frac{1}{a}+\frac{1}{b}\right]$ $(\delta \ll a, c-b)$	$\frac{1}{\pi a\delta\sigma_c}$ $(\delta \ll a)$	$\frac{2}{w\,\delta\sigma_c}$ $(\delta \ll t)$
$L\,(H/m)$	$\frac{\mu}{2\pi}\ln\frac{b}{a}$	$\frac{\mu}{\pi}\cosh^{-1}\frac{d}{2a}$	$\frac{\mu d}{w}$
$G\,(S/m)$	$\frac{2\pi\sigma}{\ln\frac{b}{a}}$	$\frac{\pi\sigma}{\cosh^{-1}\frac{d}{2a}}$	$\frac{\sigma w}{d}$
$C\,(F/m)$	$\frac{2\pi\varepsilon}{\ln\frac{b}{a}}$	$\frac{\pi\varepsilon}{\cosh^{-1}\frac{d}{2a}}$	$\frac{\varepsilon w}{d}$ $w \gg d$

Table 2.1: parameters formula of the three types of TL illustrated in figure 2.3 [5].

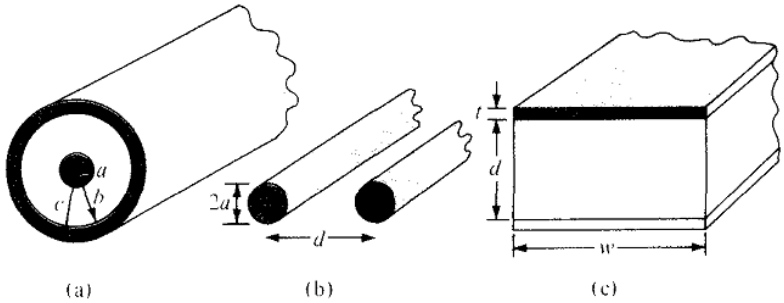

Figure 2.3: Common TLs [5]: (a) coaxial line, (b) two-wire line, (c) planar line.

2.3 TL Equations

To solve the TL equation consider the TL connecting the source to the load as shown in figure 2.4, and that TL has an equivalent circuit as shown in figure 2.5 for the portion of length Δz of TL. By applying Kirchhoff's voltage law and Kirchhoff's current law in the circuit in figure 2.5, we obtain equation 2.1 and 2.2 respectively.

$$-\frac{\mathrm{V}(\mathrm{z}+\Delta\mathrm{z},\mathrm{t})-\mathrm{V}(\mathrm{z},\mathrm{t})}{\Delta\mathrm{z}}=R\,I(z,t)+L\,\frac{\partial\mathrm{I}(\mathrm{z},\mathrm{t})}{\partial\mathrm{t}}, \tag{2.1}$$

$$-\frac{\mathrm{I}(\mathrm{z}+\Delta\mathrm{z},\mathrm{t})-\mathrm{I}(\mathrm{z},\mathrm{t})}{\Delta\mathrm{z}}=GV(\mathrm{z}+\Delta\mathrm{z},t)+C\,\frac{\partial\mathrm{V}(\mathrm{z}+\Delta\mathrm{z},\mathrm{t})}{\partial\mathrm{t}}. \tag{2.2}$$

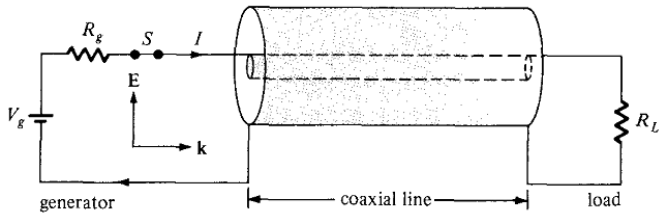

Figure 2.4: Coaxial line connecting the generator to the load [5].

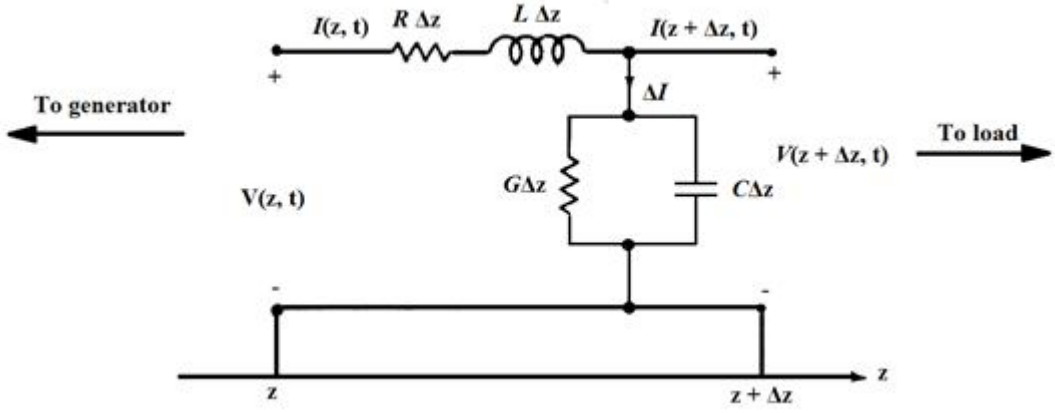

Figure 2.5: The equivalent circuit model of an infinitesimal length Δz of a two conductor TL [5].

On the limit $\Delta z \to 0$, equations 2.1 and 2.2 will be,

$$-\frac{\partial\mathrm{V}(\mathrm{z},\mathrm{t})}{\partial\mathrm{z}}=R\,I(\mathrm{z},\mathrm{t})+L\,\frac{\partial\mathrm{I}(\mathrm{z},\mathrm{t})}{\partial\mathrm{t}}, \tag{2.3}$$

$$-\frac{\partial\mathrm{I}(\mathrm{z},\mathrm{t})}{\partial\mathrm{z}}=GV(\mathrm{z},\mathrm{t})+C\,\frac{\partial\mathrm{V}(\mathrm{z},\mathrm{t})}{\partial\mathrm{t}}. \tag{2.4}$$

If we assume $V(z, t)$ and $I(z, t)$ are a harmonic time dependence, $V_s(z)$ and $I_s(z)$ are the phasor forms of $V(z, t)$ and $I(z, t)$ respectively; therefore, we may write $V(z, t)$ and $I(z, t)$ in the following forms

$$V\left(z,t\right)=Re\left[V_s\left(z\right)e^{jwt}\right], \tag{2.5}$$

$$I\left(z,t\right)=Re\left[I_S\left(z\right)e^{jwt}\right]. \tag{2.6}$$

From equations (2.3-2.6), we have

$$\frac{dV_s}{dz}=-\left(R+j\omega L\right)I_s=-Z'I_s, \tag{2.7}$$

$$\frac{dI_s}{dz}=-\left(G+j\omega C\right)V_s=-Y'V_s, \tag{2.8}$$

where Z' and Y' are a series impedance and a shunt admittance respectively per unit Length. By taking the second derivative of V_s and I_s, we obtain

$$\frac{d^2V_s}{dz^2}=\gamma^2V_s, \tag{2.9}$$

$$\frac{d^2I_S}{dz^2}=\gamma^2I_s, \tag{2.10}$$

$$\gamma=\sqrt{\left(R+j\omega L\right)\left(G+j\omega C\right)}=\alpha+j\beta, \tag{2.11}$$

where γ is a propagation constant (in per meter), α is the attenuation constant (in nepers per meter), and β is the phase constant (in radian per meter). The solution of these equations is in the form of waves in the $+z$ and $-z$ direction, which for sinusoidal excitation take the form of V_s and I_s as follows,

$$V_s=V_o^+\,e^{-\gamma z}+V_o^-\,e^{\gamma z}, \tag{2.12}$$

$$I_s=I_o^+\,e^{-\gamma z}+I_o^-\,e^{\gamma z}, \tag{2.13}$$

where V_o^+, V_o^-, I_o^+, and I_o^- are wave amplitudes; the + and – signs denotes for wave traveling along $+z$ and $-z$ directions.

The characteristic impedance of a TL Z_o is the ratio of the amplitudes of voltage and current of a single wave propagating along the line; that is, a wave travelling in one direction in the absence of reflections in the other direction [5].

$$Z_o=\frac{V_o^+}{I_o^+}=-\frac{V_o^-}{I_o^-}=\sqrt{\frac{\left(R+j\omega L\right)}{\left(G+j\omega C\right)}}=\sqrt{\frac{Z}{Y}} \tag{2.14}$$

3- Metamaterials

3.1 Introduction

Metamaterial (MTM) have attracted much attention of scientists due to their vital applications. These materials are promising towards the development of communications because they exhibit controllable electromagnetic properties. The MTM are usually arranged in periodic patterns or quasi-periodic structures.

There have been various definitions of electromagnetic metamaterials, where Walser from the University of Texas at Austin, defined the term ‘‘metamaterial’’ [6] as "*achieve material performance beyond the limitations of conventional composites*.". While Metamorphose, the European Network of Excellence, terms the metamaterials as "*Metamaterials exhibit multi-functional characteristics that can be engineered to satisfy prescribed requirements*" [7].

3.2 A Historical Overview of Electromagnetic Metamaterials

Permittivity (ε) and permeability (μ) are two parameters used to characterize the magnetic and electric properties of materials interacting with electromagnetic fields. The *permittivity* of a medium describes how much electric field is generated per unit charge in that medium, while *Permeability* is the measure of the ability of a material to support the formation of a magnetic field within itself. Most of the materials in nature have positive permittivity and permeability where referred to double-positive media (DPS). In contrast, if both of permittivity any permeability are negative they are called double-negative (DNG) and are also referred to *as Metamaterial* or LHMs. Materials with one negative parameter are named single-negative (SNG), and classified into two subcategories, namely epsilon-negative (ENG) if the media have negative permittivity, and mu-negative (MNG) if the media have negative permeability. The four different kinds of materials are displayed in figure 3.1. In the nature there are ENG materials such as cold plasma and silver at microwave and optical frequencies, respectively, and ferromagnetic materials exhibit a negative permeability behavior in the VHF and UHF regimes. However, up to date DNG material does not exist in nature and they must be created artificially.

The exposition of the four type of media according to μ and ε can deduced from the study of the equations describing the propagation of electromagnetic waves in media equations (3.1-3.2) [2]:

$$n^2 = \varepsilon\mu\,, \tag{3.1}$$

$$\beta^2 = \frac{\omega^2}{c^2} n^2\,, \tag{3.2}$$

where β is the propagation constant and n is the refractive index. If the substances have different sign for ε and μ and exhibit imaginary values of β and n. These media are not considered propagating media. However, if the two parameters ε and μ have the same sign, both β and n are real and the medium allows the propagation of electromagnetic waves.

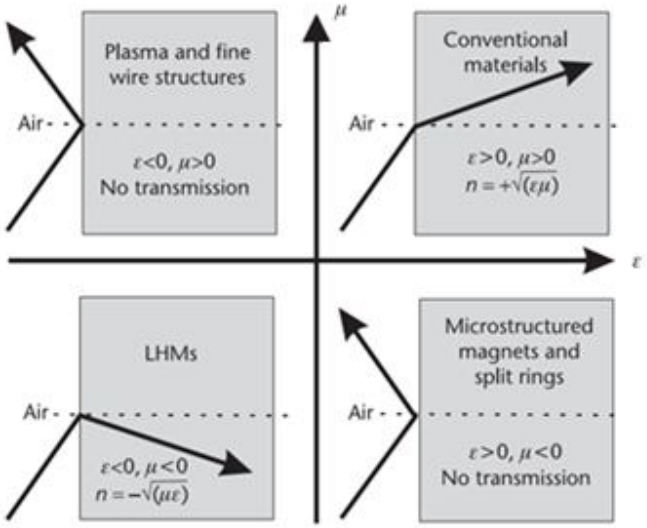

Figure 3.1: Possible domains of electromagnetic materials and wave refraction or reflection directions based on the signs of permittivity and permeability [7].

3.3 Metamaterial structure

DNG materials are not available in nature. However, the artificial synthesis of such media need to made media with both permittivity and permeability are negative. Rodded medium and SRR medium have been used as essential components to create LHMs. Rodded medium is a very interesting example of artificial media ENG. Rodded medium is formed by a regular lattice of conducting wires with radii as shown in figure 3.2. Permittivity for the wires medium is negative over a very wide frequency range. On the other hand, The SRRs are more widely used to possess negative permeability media to made artificial MNG [7].

The thin wires array shown in figure 3.2 can be expressed their effective permittivity in the form [8]:

$$\varepsilon_{eff} = 1 - \frac{\omega_p^2}{\omega^2}, \tag{3.3}$$

$$\omega_p^2 = \frac{2\pi c^2}{a^2 \ln(a/r)}, \tag{3.4}$$

where ω_p is the plasma frequency, ω is the frequency of the incident electromagnetic wave, a is the lattice parameter of the wire array, r is the radius of a wire, and c is the speed of light in vacuum. From this point, there is negative permittivity effect in the thin wires array when ω is less than ω_p.

A plasmon is defined as "quantum of plasma oscillation." [9] typically, plasmons are excited by scattering an electron off the plasma, and measuring the energy lost by the electron [9].

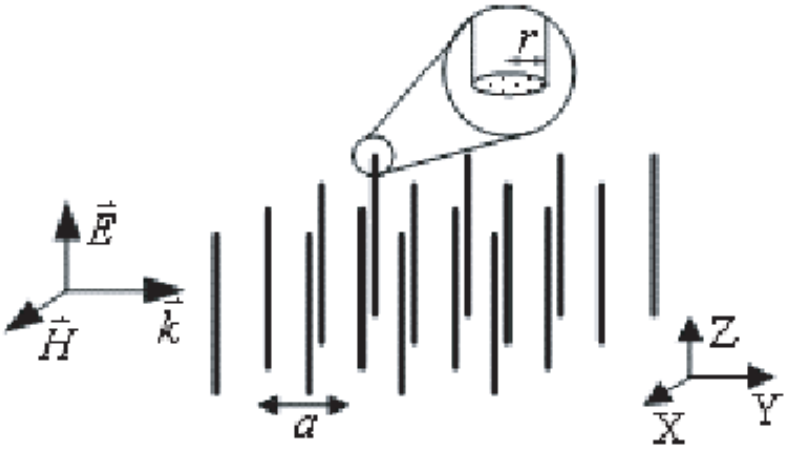

Figure 3.2: The geometry of wire medium [8].

The SRR is formed by two split metallic rings united center, as shown in figure 3.3. When we excite time-varying magnetic field in the *z* direction of SRR, the split in rings force the current to flow as displacement current between them. The closed current loop produce capacitance between the inner and the outer ring, which leads to a resonance which can be modeled as is shown in figure 3.3 [2].

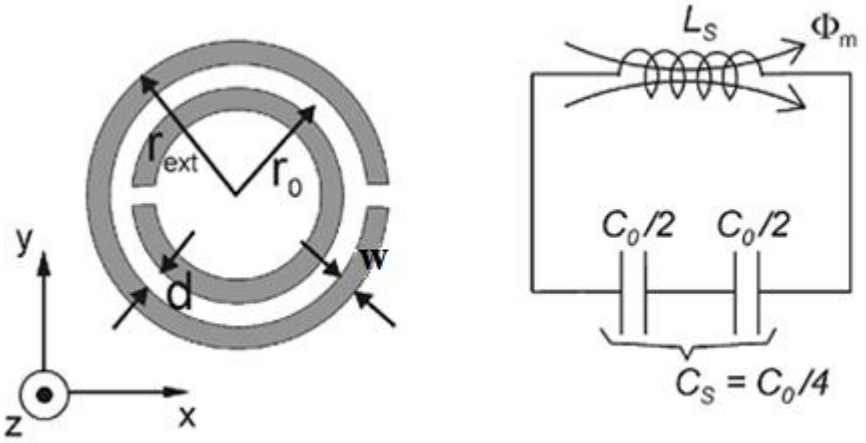

Figure 3.3: SRR and its equivalent circuit [2].

Figure 3.3 shows the modeling of SRR, where L_s is the resonator self-inductance, can be approximated by that of a single ring with averaged radius r_0, where C_0 stands for the total capacitance between the rings, C_0 can be obtained as $C_0=2\pi r_0 C_{pul,}$ where C_{pul} is capacitance per unit length between the rings. The resonance frequency of the SRR is given by equation 3.5 [2].

$$\omega_o = \frac{1}{\sqrt{C_s L_s}}, \tag{3.5}$$

where C_s is the series capacitance of the upper and lower parts of SRR.

The effective permeability of such a medium can be estimated as:

$$\mu_{eff} = 1 - \frac{F\omega^2}{\omega^2 - \omega_0^2}, \tag{3.6}$$

where F is the fractional area occupied by the interior of the resonator within the unit cell [10]:

$$F = \frac{\pi r^2}{a^2}, \tag{3.7}$$

where r is the radius of the inner ring, a is the unit-cell dimension in the xy plane. on the other hand, we can calculate ω_0 by geometric parameters from [10]:

$$\omega_0 = \frac{3ac^2}{\pi \ln(\frac{2w}{d} r^3)}, \tag{3.8}$$

where d is the gap between inner and outer ring and w is the ring width.

The variation of μ_{eff} around the resonance frequency is shown in figure 3.4. Just above ω_0 and up to ω_{mp} (the "magnetic plasma frequency"), the effective permeability is negative, which works as MNG effective media.

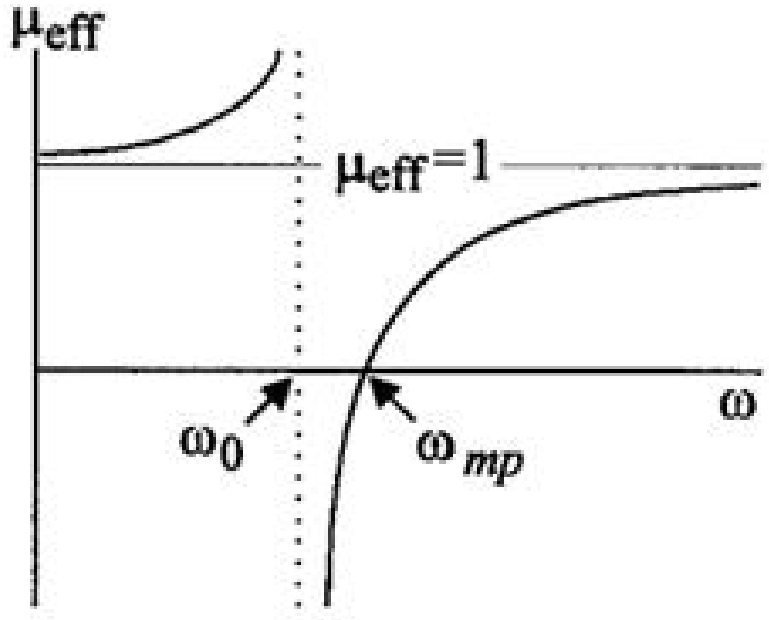

Figure 3.4: Effective magnetic permeability of a MNG medium [11].

3.4 Complementary Split-Rings Resonators

On the basis of the SRR, numerous sub-wavelength resonators with similar topologies have been proposed. One of them is the complementary split-ring resonator

(CSRR) as show in Figure 3.5(a) . In this case, the rings forming the resonator are etched on a metallic surface. This occurs in such a way that, both structures have the same resonance frequency, but, contrary to the SRR, the CSRR exhibits negative values of the dielectric permittivity around its resonance, which can be excited by means of an axial electric field.

The intrinsic circuit model for the CSRR is shown in Figure 3.5(b). In this circuit, the inductance L_S of the SRR model is substituted by the capacitance C_c of a disk of radius $r_0 - w/2$. Conversely, the series connection of the two capacitances $C_0/2$ in the SRR model is substituted by the parallel combination of the two inductances connecting the inner disk to the ground. Each inductance is given by $L_0/2$, where $L_0=2\pi r_0 L_{pul}$ and L_{pul} is the per unit length inductance of the coplanar waveguide connecting the inner disk to the ground [2].

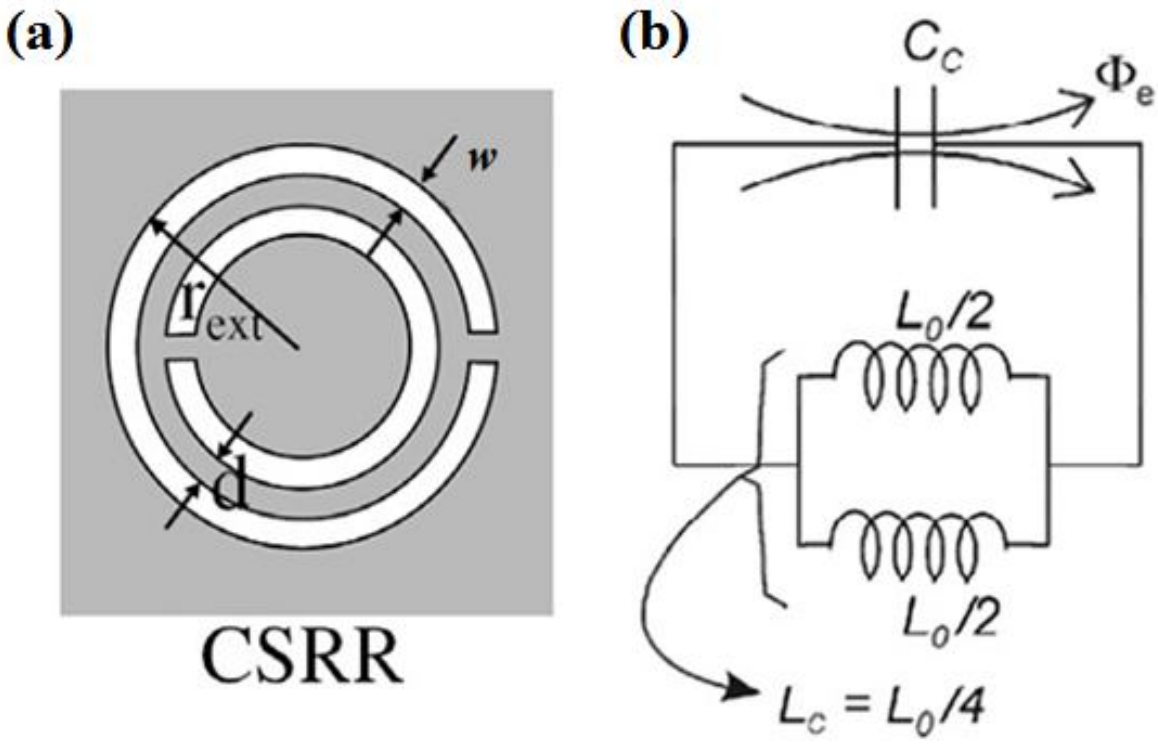

Figure 3.5 [2]: (a) CSRR. (b) CSRR equivalent circuit.

3.5 Left-Handed Media

When we talked about the metamaterials we said that these materials are not available in nature, where this material taking negative values for the magnetic permeability and the dielectric permittivity simultaneously. Another name for the metamaterials are a left-handed media (LHM). Considering a plane wave, we can write equations (3.9) and (3.10) [7] where K is wave vector, H is a magnetic field vector, and E is an electric field vector.

$$\vec{K} X \vec{E} = \omega\mu \vec{H} \ , \tag{3.9}$$

$$\vec{K} X \vec{H} = -\omega\varepsilon \vec{E} \ . \tag{3.10}$$

Form equations 3.9 and 3.10 if ε >0 and μ >0, the orthogonal *K*, *E*, and *H* are RH as shown in figure 3.6(a). Whereas when both ε and μ are negative, the vector system is left-handed as shown in figure 3.6(b). This is the reason why these media are called "left-handed media".

Whereas the wave vector reverses its direction in LHM, the Poynting vector keeps its direction in LHM and RHM.

$$\vec{S} = \vec{E} \, x \, \vec{H} \tag{3.11}$$

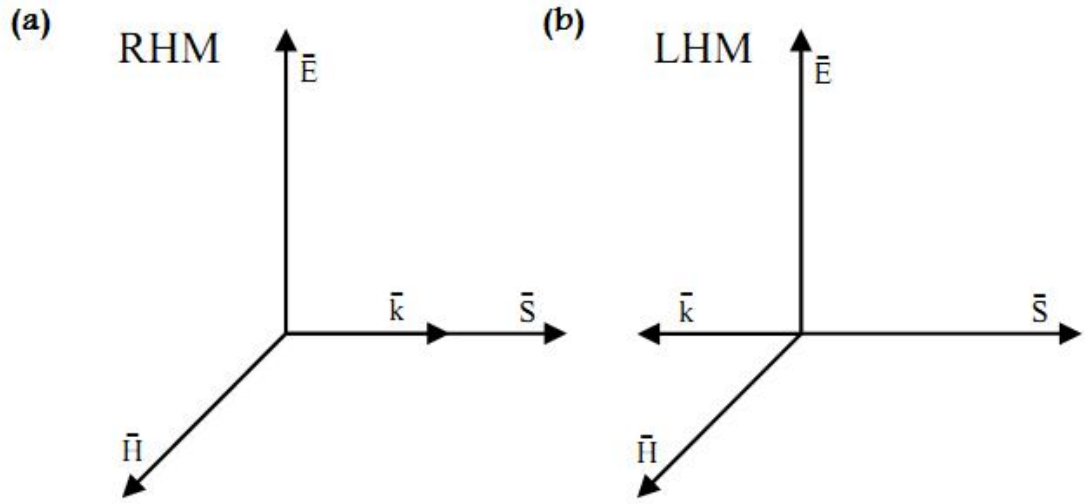

Figure 3.6: Representation of the field, wave and Poynting vectors for propagating waves [2]: (a) LHM, (b)LHM.

So the energy flux and the wave fronts travel in opposite directions or, in other meaning, in LHM the group and the phase velocities are antiparallel (backward propagation).

In LHM, we can express the two negative magnitudes, ε and μ, in polar coordinates; thus, equation (3.1) can be rewritten as follows [7] :

$$n = \sqrt{-\varepsilon}\sqrt{-\mu} = \sqrt{e^{j\pi}\varepsilon}\sqrt{e^{j\pi}\mu} = e^{j\pi}\sqrt{\varepsilon\mu} = -\sqrt{\varepsilon\mu} \tag{3.12}$$

So the refraction index is negative in LHM media. As a consequence, when a wave arrives to a LHM through a RHM the refraction angle is also negative as shown in figure 3.7.

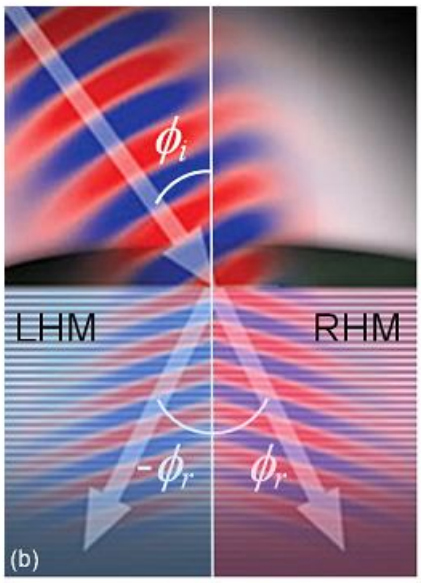

Figure 3.7: Reflection index wave arrives to a LHM through a RHM [7].

4 - Composite Left/Right handed Transmission

4.1 Introduction

There are two main approaches devoted to the implementation of artificial TLs and their application in microwave device design: the CL-loaded TL and the resonant-type approach

The TL approach to implement LHM was first introduced by a group at university of Toronto in 2002 [12]. The approach is based on the mapping of the electric and magnetic field in the media to the voltage and currents of the equivalent distributed L-C network. Where the dielectric properties like permittivity and permeability can be modeled using distributed L-C networks.

LHM TLs implemented in coplanar, strip line and microstrip technologies [2] are more suitable for microwave device design. The big advantages of these artificial TLs are their design flexibility and compact dimensions, given that phase and characteristic impedance can be tunable to some extent in order to obtain the suitable properties that each design requires.

The second main type of approach artificial TLs with LH characteristics is the resonant-type approach based on sub-wavelength resonators. Since this type of approach depending on the resonators as SRR-based TL makes them useful in microwave device design. The different type of resonator make different type of applications developed by metamaterial TLs such as filters, power dividers or hybrid couplers, among others

4.2 TL implementation of LHM

In chapter 2, the propagation characteristics in the normal TL (RH-TL) is explained. We will make an analogy between RH-TL and LH-TL to study the propagation characteristics in both media. We will use the equivalent T-circuit model of the TL to model both of TL-media as shown in figure 4.1, where the series impedance and the shunt admittance Z and Y can be matched with the magnitudes ε_{eff} and μ_{eff} (Z' and Y' per-unit-length magnitudes): [2]

$$Z' = j\omega\mu_{eff}\,, \tag{4.1}$$

$$Y' = j\omega\varepsilon_{eff}\,. \tag{4.2}$$

The sign of Z' and Y' may be positive or negative depending on the sign of μ_{eff} and ε_{eff}. Therefore, there are four possibilities of Z' and Y' as indicated in table 4.1. The sign of Z' and Y' determines the propagating or not propagating nature of the line. Where the propagation can be exist when both of Z' and Y' have the same sign.

Therefore, considering lossless RH-TL, modeled by series inductances and shunt capacitances as shown in figure 4.2 (a), exhibits positive values of ε_{eff} and μ_{eff}.

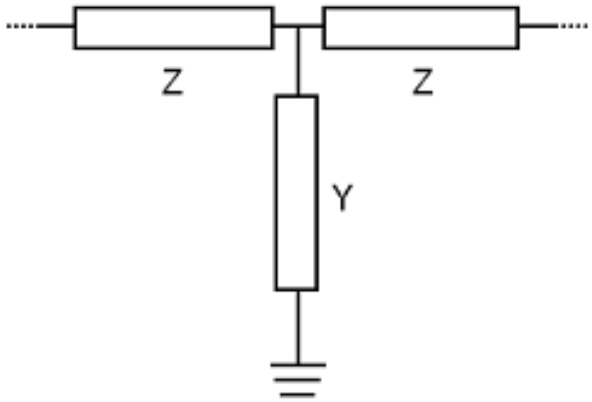

Figure 4.1: T-circuit model of the TL [2].

Impedances		Medium	Propagating
$Z' = \left(\sim \mu_{eff} \right)$	$Y' = \left(\sim \varepsilon_{eff} \right)$		
>0	>0	Conventional TL. DPS	YES
>0	<0	SNG	NO
<0	>0	SNG	NO
<0	<0	Dual TL DNG	YES

Table 4.1: Variation of TLs properties with the sign of the impedances [2].

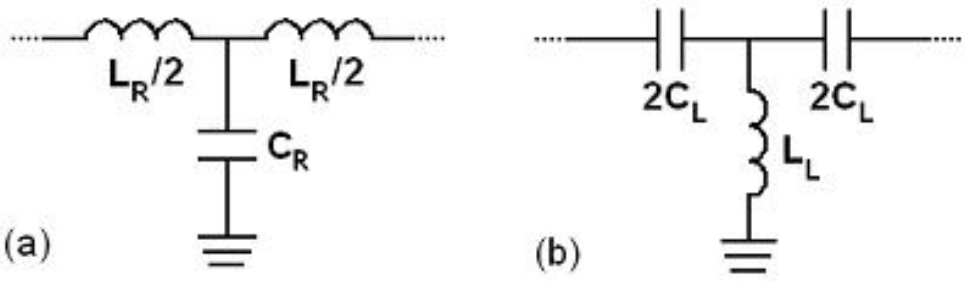

Figure 4.2: (a) Unit cell for a RH TL. (b) Unit cell for a LH TL [2].

$$\mu_{eff} = \frac{L_R}{2l} = \frac{L_R^{'}}{2}, \tag{4.3}$$

$$\varepsilon_{eff} = \frac{C_R}{l} = C_R^{'}, \tag{4.4}$$

where l is the length of the unit cell.

Inserting equations 4.3 and 4.4 into equations 4.1 and 4.2, we will get the right hand impedance (Z_R) and admittance (Y_R) as follows,

$$Z_R = j\omega\frac{L_R}{2}, \tag{4.5}$$

$$Y_R = j\omega C_R \tag{4.6}$$

On the contrary, in LH-TL we obtain negative values for ε_{eff} and μ_{eff}, so Z_L must be capacitive, and Y_L must be inductive as shown in figure 4.2(b). ε_{eff} and μ_{eff} are obtained by [2]:

$$\mu_{eff} = \frac{-1}{\omega^2 2C_L l}, \tag{4.7}$$

$$\varepsilon_{eff} = \frac{-1}{\omega^2 L_L l}, \tag{4.8}$$

$$Z_L = \frac{1}{j\omega 2C_L}, \tag{4.9}$$

$$Y_L = \frac{1}{j\omega L_L}. \tag{4.10}$$

From our lossless T-network (figure 4.1) we can drive the phase constant β, characteristic impedance Z_o, phase velocities v_p, and group velocities v_g for both RH-TL and LH-TL [2].

The propagation constant can be obtained from Z and Y

$$\cos\beta l = 1 + ZY, \tag{4.11}$$

$$\beta = \pm\sqrt{-2Z'Y'}. \tag{4.12}$$

The characteristic impedance can be obtained as:

$$Z_0 = Z_B = \sqrt{Z\left(\frac{2}{Y} + Z\right)}. \tag{4.13}$$

Phase and group velocities are given by the following expressions:

$$v_p = \frac{\omega}{\beta}, \tag{4.14}$$

$$v_g = \frac{\partial\omega}{\partial\beta}. \tag{4.15}$$

For RH-TL, from the equations 4.5 and 4.6, we can obtain the following characteristic impedance,

$$Z_{B_R} = \sqrt{\frac{L_R}{C_R}\left(1-\omega^2\frac{L_R C_R}{4}\right)}, \tag{4.16}$$

and propagation constant is

$$\beta_R = +\omega\frac{\sqrt{L_R C_R}}{l} = \omega\sqrt{L_R^{'}C_R^{'}}\ , \tag{4.17}$$

moreover, the phase and group velocities are:

$$v_{p_R} = \frac{\omega}{\beta} = +\sqrt{\frac{1}{L_R^{'}C_R^{'}}}\ , \tag{4.18}$$

$$v_{g_R} = \frac{\partial\omega}{\partial\beta} = +\sqrt{\frac{1}{L_R^{'}C_R^{'}}} = v_p\ , \tag{4.19}$$

on the other hand, for the LH-TL from equations 4.9 and 4.10, we get

$$Z_{B_L} = \sqrt{\frac{L_L}{C_L}\left(1-\frac{1}{\omega^2 4L_L C_L}\right)}, \tag{4.20}$$

$$\beta_L = -\sqrt{-2Z_L^{'}Y_L^{'}} = -\frac{1}{\omega l\sqrt{C_L L_L}}, \tag{4.21}$$

$$v_{p_L} = \frac{\omega}{\beta} = -\omega^2 l\sqrt{C_L L_L}\ , \tag{4.22}$$

$$v_{g_L} = \frac{\partial\omega}{\partial\beta} = +\omega^2 l\sqrt{C_L L_L}\ . \tag{4.23}$$

From previous equation we note that the sign of phase velocity and propagation constant is different in both of RH-TL and LH-TL. In the RH-TL the sign of phase velocity and propagation constant are positive confirms forward propagation in RH-TL. In opposite to the RH-TL, the sign of phase velocity and propagation constant are negative confirms backward propagation in LH-TL. In the other word, the sign of the propagation constant has been chosen in order to guarantee a positive value of the group velocity and negative value of the phase velocity in LH-TL [2]. The dispersion diagrams and the characteristic impedance of the RH-TL and the dual LH-TL are depicted in figure 4.3, where

$$\omega_{CR} = \frac{2}{\sqrt{L_R C_R}} \tag{4.24}$$

$$\omega_{C_L} = \frac{1}{2\sqrt{L_L C_L}} \tag{4.25}$$

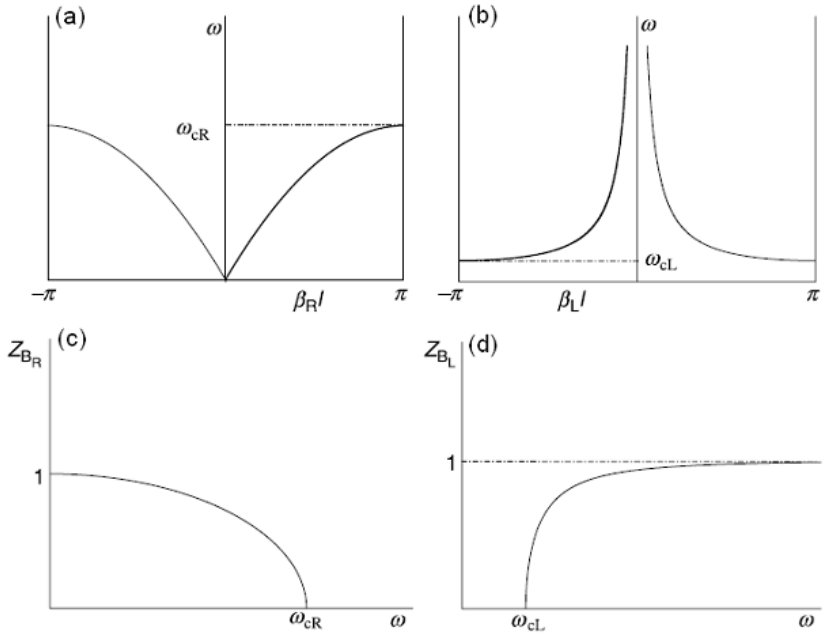

Figure 4.3 [2]: (a) Dispersion diagrams for a RH TL. (b) Dispersion diagrams for a LH TL. (c) Normalize characteristic impedances for a RH TL. (d) Normalize characteristic impedances for a LH TL.

4.3 Composite Right/Left handed TL

As shown in the previous section, the pure LH-TL modeled by series capacitances and shunt inductances as shown in figure 4.2 (b). However, this model of pure LH-TL is not possible. The implementation of LH-TL requires a host conventional TL (RH-TL) with shunt capacitances and series inductances. The host can be applied with different kinds of TLs, such as microstrip and coplanar waveguides (see figure 4.4(a)). These hosts do not allow to obtain a pure LH-TL, since the host medium introduces L_R and C_R will take part in the structure of the TL as shown in figure 4.4(b)

At low frequencies, the loading element (LH components L_L, C_L) are dominating, so the propagation characteristics of the TL act as pure LH-TL. While, at high frequencies the host element (RH components L_R, C_R) are dominating, so the propagation characteristics of the TL act as pure RH-TL. The composite behavior of these TLs is known as composite right-left handed (CRLH) TLs or (CRLH-TL), and the design of CRLH-TL is called CL-loaded TLs.

In the previous section, we drive the values of ε_{eff} and μ_{eff} of the RH and LH TL. In a similar way, the expressions of ε_{eff} and μ_{eff} are [13]

$$\mu_{eff} = \frac{L_R}{2l} - \frac{1}{\omega^2 2C_L l} \tag{4.26}$$

$$\varepsilon_{eff} = \frac{C_R}{l} - \frac{1}{\omega^2 L_L l} \tag{4.27}$$

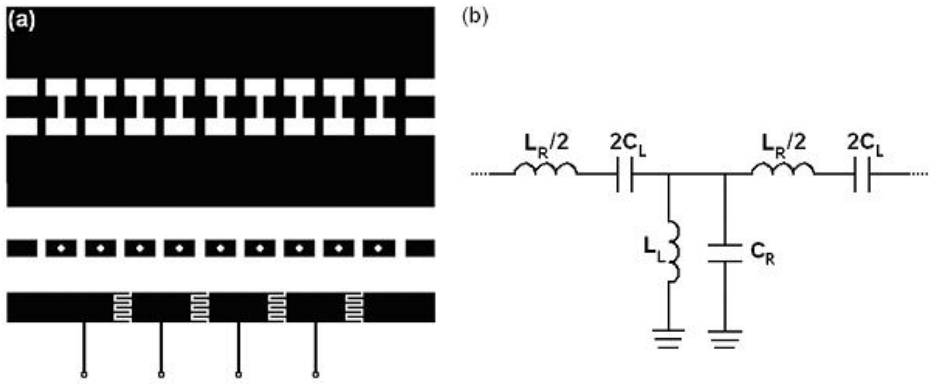

Figure 4.4 [2]: (a) Layouts of different kinds of CL-loaded TLs. From up to down: Coplanar waveguide with capacitive gaps and shunt connections, microstrip line with capacitive gaps and vias to ground and, finally, microstrip line with interdigital capacitors and shunt-connected inductive stubs (b) T-circuit model of a composite right-left handed TL (CRLH TL).

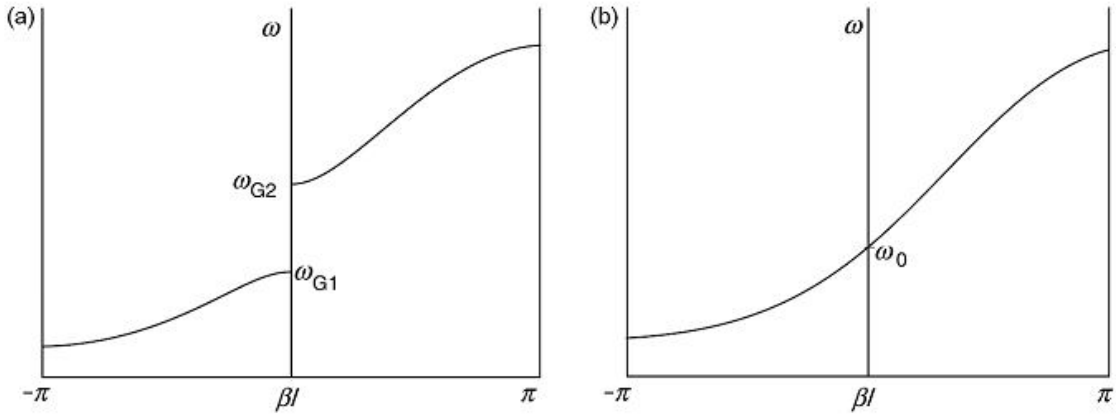

Figure 4.5 [2]: (a) Dispersion diagram of a non-balanced CRLH TL, (b) Dispersion diagram of a balanced CRLH TL.

Both ε_{eff} and μ_{eff} can be positive or negative, where their values depend on the frequency, at high frequencies both ε_{eff} and μ_{eff} are positive so the TL acts as RH-TL, while at low frequencies both ε_{eff} and μ_{eff} are negative so the TL acts as LH-TL. At certain frequency range known as frequency gap both ε_{eff} and μ_{eff} have different signs where transmission is not allowed as shown in figure 4.5(a). The frequency gap starts from ω_{G1} and ends at ω_{G2}. The LH behaviors below the ω_{G1} and RH behaviors above the ω_{G2} and no transmission allowed between ω_{G1} and ω_{G2}. The values of both ω_{G1} and ω_{G2} depend on the values of the capacitance and inductance. The values of ω_{G1} and ω_{G2} are functions of the resonance frequencies of the series branche (ω_s) and shunt branche (ω_p):

$$\omega_{G1} = \min\left(\omega_s, \omega_p\right) \quad , \quad \omega_{G2} = \max\left(\omega_s, \omega_p\right) \tag{4.28}$$

At the balanced case the resonance frequencies of the series and shunt branches must be equal. In addition, their values must equal to ω_0. At this frequency, the frequency gap is forced to disappear as shown in figure 4.5(b) where ω_o is defined as:

$$\omega_0 = \frac{1}{\sqrt{L_L C_R}} = \frac{1}{\sqrt{L_R C_L}} \ . \tag{4.29}$$

4.4 Resonant-type Metamaterial TLs

After appearance of CL-loaded TL to approach artificial transmission lines with left-handed characteristics, a new type of approach left-handed characteristics based on sub-wavelength resonators came out. The dependence of this new type at transmission lines on the resonators such as SRR-based transmission line makes them especially interesting and useful in microwave device design. New kinds of resonators had several types of applications are developed and applied to metamaterial transmission lines such as filters, power dividers or hybrid couplers, among others.

The most two famous resonator to impalement artificial left-handed are SRRs and CSRRs. These types of resonators are hosted on conventional TL as mounted element, the effect of hosting TL appears at specific frequency band where the series and shunt reactances make the behavior of the TL acts as RHTL while in other specific frequency band the series and shunt reactances make the behavior of the TL act as LHTL.

The sub-wavelength dimensions of the resonators allow the synthesis of very compact structures with significant design flexibility and make them suitable for microwave device miniaturisation [2].

The excitation of SRR-type resonators are different from the excitation of CSRR-type resonators. While the SRR is excited by an axial magnetic field, CSRR is excited by an axial electric field. This allows different kinds of coupling for each kind of resonator. SRRs can be coupled to a coplanar waveguide by locating them on the bottom side of the substrate, while the CSRRs, they can be etched on the ground plane under a microstrip line, or they can be etched on the metallic strip in both, microstrip and coplanar TLs. [2].

In the following section we will expose two types to approach the resonator in the TL: purely resonant approach and hybrid approach. The focus of our work is on the CSRR-type TLs in the hybrid approach, which have been mainly studied and applied in our design.

4.4.1 Purely Resonant Approach

The purely resonant approach is divided into two resonator types SRR and CSRR resonant .

4.4.1.1 Purely SRR Resonant Approach

The Metamaterial TL is based on a resonator which consists of coplanar waveguide, SRRs and shunt-connect metallic strips [2]. The SRRs resonator is

magnetically coupled with coplanar waveguide, where the SRRs located on the bottom side of substrate as shown in figure 4.6(a). The metallic strip with SRRs acting as shunt inductance around the resonance frequency of the SRRs, at this condition the TL behavior as LH-TL where the shunt reactance is inductive and series reactance is capacitive. The equivalent circuit model of the TL shown in figure 4.6(b), which can be simplified to the π-circuit shown in figure 4.6(c) [2].

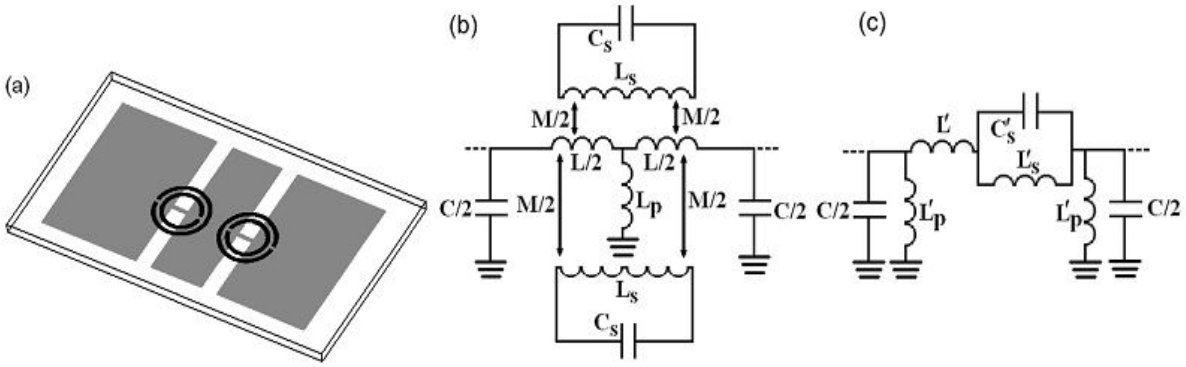

Figure 4.6 [2]: (a) Scheme of a unit cell of the first SRR resonant-type metamaterial TL. (b) Recently proposed improved circuit model for the structure shown in (a). (c) Modified circuit model for the structure shown in (a).

In figure 4.6(b), C_s and L_s model the SRRs which are magnetically coupled with coplanar waveguide through mutual inductance M, to obtain a series capacitive element in modeling circuit [2]. While the metallic strips are modeled by L_p to get a shunt inductance in the model. The series capacitive (Cs) and shunt inductance (L_p) are the essential elements to LH behavior. The inductance and capacitance of the waveguide are model by L and C respectively, where L and C are represented the RH behavior. The transformation from (b) to (c) satisfy the following equations [2]:

$$L_S^{'} = 2M^2 C_s \omega_0^2 \frac{\left(1+\frac{L}{4L_p}\right)^2}{1+\frac{M^2}{2L_pL_s}}, \tag{4.30}$$

$$C_S^{'} = \frac{L_s}{2M^2\omega_0^2}\left(\frac{1+\frac{M^2}{2L_pL_s}}{1+\frac{L}{4L_p}}\right)^2, \tag{4.31}$$

$$L' = \left(2+\frac{L}{2L_p}\right)\frac{L}{2} - L_S^{'}, \tag{4.32}$$

$$L_P^{'} = 2L_p + \frac{L}{2}. \tag{3.33}$$

The series and shunt impedances Z_s and Z_p, are respectively given by,

$$Z_s = j\omega\left(L' + \frac{L_S'}{(1-\omega^2 L_S' C_S')}\right), \tag{4.34}$$

$$Z_p = j\,\omega\frac{L_P'}{1-\omega^2 L_P'\dfrac{C}{2}}\,. \tag{4.35}$$

The sign of Z_s and Z_p change according to the value of the frequency. At low frequency $\chi_s<0$ and $\chi_p>0$, left handed propagation appears; however, at high frequency $\chi_s>0$ and $\chi_p<0$, RH propagation occurs, where χ_s and χ_p are the imaginary parts of Z_s and Z_p respectively.

The dispersion relation of the line can be written as:

$$\cos\beta l = 1+\frac{Z_s}{Z_p}\,, \tag{4.36}$$

resulting:

$$\cos\beta l = 1+\left(L' + \frac{L_S'}{(1-\omega^2 L_S' C_S')}\right)\frac{\left(1-\omega^2 L_P'\dfrac{C}{2}\right)}{L_P'}, \tag{4.37}$$

the characteristic impedance can be rewritten from equation (4.13) by transform from T-circuit model to π-circuit model:

$$Z_B = \sqrt{\frac{Z_s Z_p^2}{2Z_p + Z_s}} \tag{4.38}$$

4.4.1.2 Purely CSRR Resonant Approach

As mentioned above, The first type Metamaterial TL based on SRRs, the other type of resonator can be implemented with complementary split-ring resonators (CSRRs). The TL is implemented by etching CSRRs on the ground plane of microstrip line and capacitive gap etched on the microstrip line above the resonator as shown in figure 4.7(a). Where the CSRRs providing negative permittivity (ε) and capacitive gap providing negative permeability (μ). The figure 4.7(b) shows The equivalent circuit model of figure 4.7(a). The gap capacitance is modeled by C_g, while the CSRR is modeled by L_c and C_c where electrically coupled to the line through the capacitance C and L represents the line inductance.

Figure 4.7(c) shows the new equivalent circuit model of structure figure 4.7(a). Which provides a better description of the physical behavior. The new model is able to explain the importance of the coupling capacitance C when a capacitive gap is present or not. Where modelling the gap as a π-circuit formed by the series capacitance C_s and two shunt fringing capacitances, C_f [14]. The line capacitance, C_L, and C_f form the parallel capacitance C_{par}

$$C_{par} = C_f + C_L \tag{4.39}$$

$$2C_g = 2C_s + C_{par} \tag{4.40}$$

$$C = \frac{C_{par}\left(2C_s + C_{par}\right)}{C_s} \tag{4.41}$$

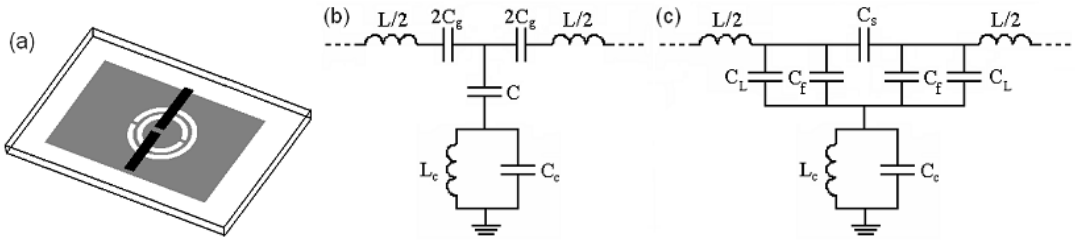

Figure 4.7 [2]: (a) A unit cell of Purely CSRR Resonant-type metamaterial TL. (b) Equivalent T-circuit model of the structure shown in (a). (c) Recently-proposed improved circuit model for the structure shown in (a).

From the preceding equations we see that both C_g and C depend on C_s and C_{par}. This means that any changes on the capacitive gap, modifies C and Cg and their related parameters [2].

The series and shunt impedances of the T-circuit model are:

$$Z_s = j\omega\frac{L}{2} + \frac{1}{j\omega 2C_g} = \frac{1-\omega^2 C_g L}{j\omega 2C_g} \tag{4.42}$$

$$Z_p = \frac{1}{j\omega C} + j\omega\frac{Lc}{1-\omega 2C_c L_c} = \frac{1-\omega^2 L_c\left(C + C_c\right)}{j\omega C\left(1-\omega^2 C_c L_c\right)} \tag{4.43}$$

The phase of the unit cell can be calculated as the equation (4.36):

$$\cos\beta l = 1 + \frac{C}{C_g}\frac{\left(1-\omega^2 C_g L\right)\left(1-\omega^2 C_c L_c\right)}{1-\omega^2 L_c\left(C + C_c\right)} \tag{4.44}$$

From the above equation $\cos(\beta l) = -1$ if $Zs = -2Zp$ when the phase takes the values -180º and 0º which represent the upper and lower frequencies of the LH transmission band, and the zero-phase can occur when $Z_s = 0$ or $Z_p = \infty$ which represent series (ω_s) and shunt (ω_p) resonance frequencies [2].

$$\omega_s = \frac{1}{\sqrt{LC_g}} \tag{4.45}$$

$$\omega_p = \frac{1}{\sqrt{C_c L_c}} \tag{4.46}$$

The minimum value of these two frequencies (ω_s, ω_p) is the upper limit of the LH band while the maximum value is the lower limit for the RH band as shown in figure (4.8). The transmission zero frequency, ω_z, at which Z_p=0

$$\omega_z = \frac{1}{\sqrt{L_c\left(C + C_c\right)}} \tag{4.47}$$

The characteristic impedance can be calculated as:

$$Z_B = \sqrt{Z_s\left(2Z_p + Z_s\right)} \tag{4.48}$$

giving us:

$$Z_B = \sqrt{\frac{L}{C}\frac{\left(\omega^2 - \omega_s^2\right)}{\omega^2} + \frac{L}{C_c}\frac{\left(\omega^2 - \omega_s^2\right)}{\left(\omega^2 - \omega_p^2\right)} - \frac{L^2}{4}\frac{\left(\omega^2 - \omega_s^2\right)^2}{\omega^2}} \tag{4.49}$$

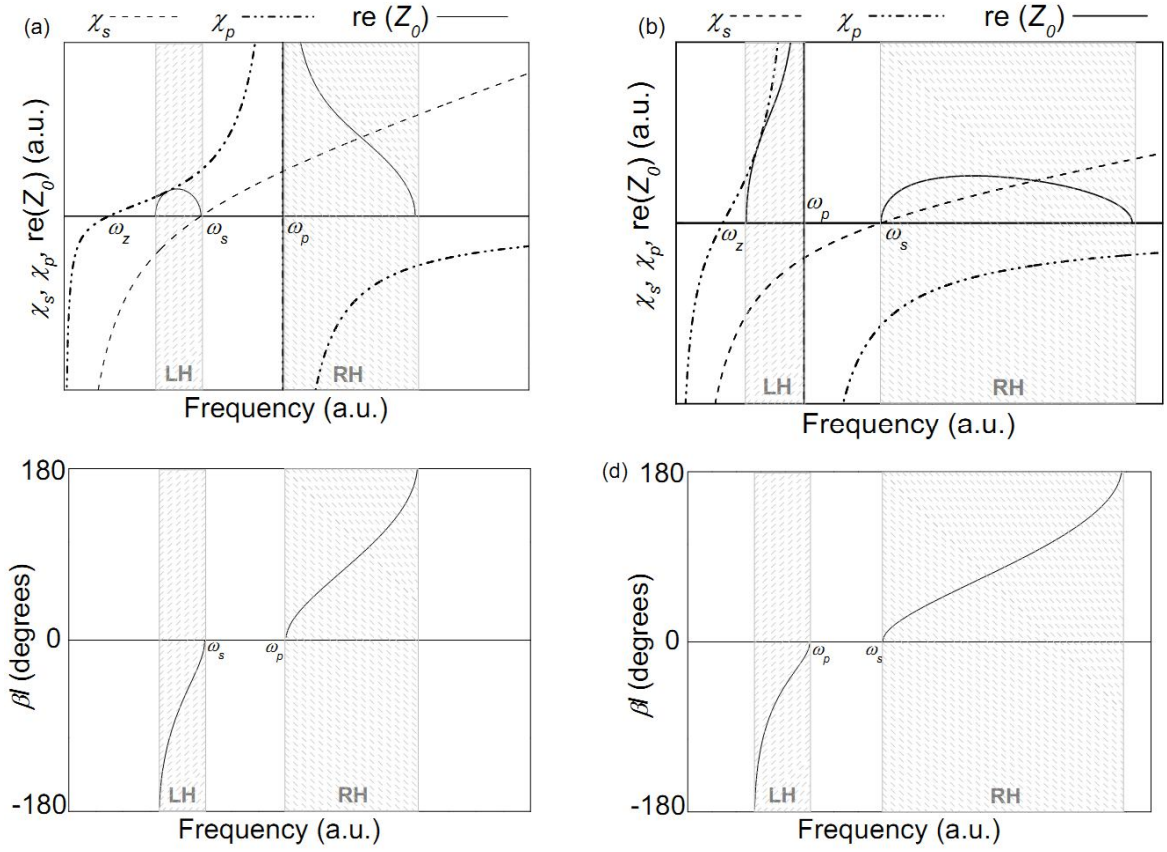

Figure 4.8: Representation of the series and shunt reactances, the characteristic impedance, and the phase (βl) for a unit cell show in figure (4.7(a)). (a) and (c) $\omega_s < \omega_p$, whereas in (b) and (d) $\omega_s > \omega_p$ [2].

The figure 4.8(c, d) show variation of the phase in the transmission bands where both, βl and Z_0, are real. When $\beta > 0$ the TL is in RH band while $\beta < 0$ TL is in LH

band. Moreover, graphs in figure 4.8(a, b) show that the LH transmission occur at $\chi s < 0$ and $\chi p > 0$, whereas in the RH transmission occur at $\chi_p < 0$ and $\chi_s > 0$.

Between the LH and RH there is a transmission gap occurred in CL-loaded TLs when there is no balance. Resonant-type TLs can be designed to be balanced by forcing ω_p and ω_s to be equal. At this case a continuous transition between both bands occurs which provides a wide transmission band with left- and right-handed depending on the frequency.

4.4.2 Hybrid Approach

Hybrid approach combines particles from CSRR, gaps and shunt inductance. The new TL composed by combining CSRRs and capacitive gaps in the purely CSRR resonant structures with the shunt inductance has new propagation characteristics as shown in figure 4.9(a). The shunt inductance contributes to obtain a negative value of permittivity that increases design flexibility to work at CRLH band and also to provide a transmission zero above the band of left-handed (figure 4.9(c)), where this transmission zero improving the rejection above the transmission band [2].

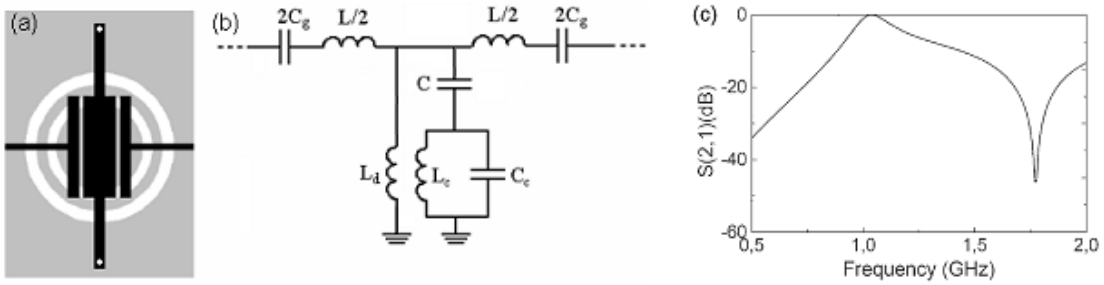

Figure 4.9 [2]: (a) unit cell of a CSRR-based hybrid unit cell. (b) Equivalent circuit model of the structure shown in (a). (c) Typical frequency response of a hybrid structure.

The equivalent circuit model and frequency response of hybrid approach shown in figure 4.9(b, c), where the CSRR are modeled by the capacitance C_c and the inductance L_c, whereas the gaps are described by the capacitance C_g. L is the inductance of the line, while the electric coupling between the line and CSRR modeled by C, and the two shunt stubs modeled by the shunt connected inductance L_d [15]. When the series reactance and shunt susceptance are both negative (LH regions), zones where they are both positive (RH bands), and intervals where they have opposite signs (no transmission bands). The utilization of the transmission zero can be guide to provide high rejection level below the main transmission band in the design of narrow band pass filters as shown in [16].

Before analysing this model, we show there are a small differences between the purely CSRR resonant approach and hybrid approach; the central stubs, shunt connected by means of vias, are modelled in the circuit by means of the shunt inductance L_d. Whereas the shunt impedance is modified to equation (4.51), the series impedance remains the same as in the purely resonant approach equation (4.50) and, thus, the series branch resonance is again given by equation (4.45). Besides the transmission zero, ω_z

equation (4.52), the new element provides a second resonance frequency for the shunt branch. The two shunt resonances are given by equations (4.53) and (4.54), where ω_r is the resonance frequency of the resonators (equation (4.55)).

$$Z_s = j\omega\frac{L}{2} + \frac{1}{j\omega 2C_g} = \frac{\left(1-\omega^2 C_g L\right)}{j\omega 2C_g} \tag{4.50}$$

$$Z_p = \left[\frac{1}{j\omega L_d} + \frac{1-\omega^2 L_c\left(C+C_c\right)}{j\omega C\left(1-\omega^2 C_c L_c\right)}\right]^{-1} \tag{4.51}$$

$$\omega_z = \frac{1}{\sqrt{L_c\left(C+C_c\right)}} \tag{4.52}$$

$$\omega_{pL} = \sqrt{\frac{\omega_r^2\left(1+L_d C\omega_z^2\right) - \sqrt{\omega_r^4\left(1+L_d C\omega_z^2\left(1+L_d C\omega_z^2\right)\right) - 4L_d C\omega_z^4\omega_r^2}}{2L_d C\omega_z^2}} \tag{4.53}$$

$$\omega_{pH} = \sqrt{\frac{\omega_r^2\left(1+L_d C\omega_z^2\right) + \sqrt{\omega_r^4\left(1+L_d C\omega_z^2\left(1+L_d C\omega_z^2\right)\right) - 4L_d C\omega_z^4\omega_r^2}}{2L_d C\omega_z^2}} \tag{4.54}$$

$$\omega_r = \frac{1}{\sqrt{C_c L_c}} \tag{4.55}$$

The diverse combinations of the position of the series resonance frequency changes with respect to the transmission zero and the shunt resonance frequencies affect the behavior of the TL. Figures 4.10 and 4.11 show some of the possible combinations. Figure 4.10(a, c) show the characteristic impedance with the series and shunt reactances and the dispersion diagrams in the case of $\omega_s < \omega_{pL} < \omega_z < \omega_{pH}$, and figure 4.10(b, d) show the characteristic impedance with the series and shunt reactances and the dispersion diagrams in the case of $\omega_{pL} < \omega_s < \omega_z < \omega_{pH}$. While the figure 4.11(a, c) show the characteristic impedance with the series and shunt reactances and the dispersion diagrams in the case of $\omega_{pL} < \omega_z < \omega_s < \omega_{pH}$, and the figure 4.11(b, d) show the characteristic impedance with the series and shunt reactances and the dispersion diagrams in the case of $\omega_{pL} < \omega_z < \omega_{pH} < \omega_s$. From these four cases. The differences of combination give rise to diverse distributions of the left and right-handed transmission bands occur flexibility for designer to select the best behaviors for his target.

The relation of the series and shunt resonate frequency make the behavior of the TLs are balance or unbalance, where at the balance case there are no transmission gap between left and right hand while at unbalance case there are gab when transition from left to right band. In contrast, let us now consider the balanced case, which more important to achieve broadband structures. Since there are two shunt resonances, there are actually two cases to achieve the balanced condition: that where the series resonance (ω_s) is equal to the lower resonance frequency (ω_{pL}) of the shunt impedance, and that case

where the series resonance (ω_s) is equal to the higher resonance frequency (ω_{PH}) of the shunt impedance. At this case, a continuous transition between the left- and right-handed band results. Since transmission zeros is located between the two shunt resonant frequency an additional band is located in the transmission band. In the case ($\omega_s = \omega_{PL}$), where are additional band above the transition frequency, in the right hand propagation. Conversely in the case ($\omega_s = \omega_{PH}$), this additional allowed band is located below the transition frequency in the LH. Nevertheless, these additional bands are typically very narrow and may not be useful in practical applications [15].

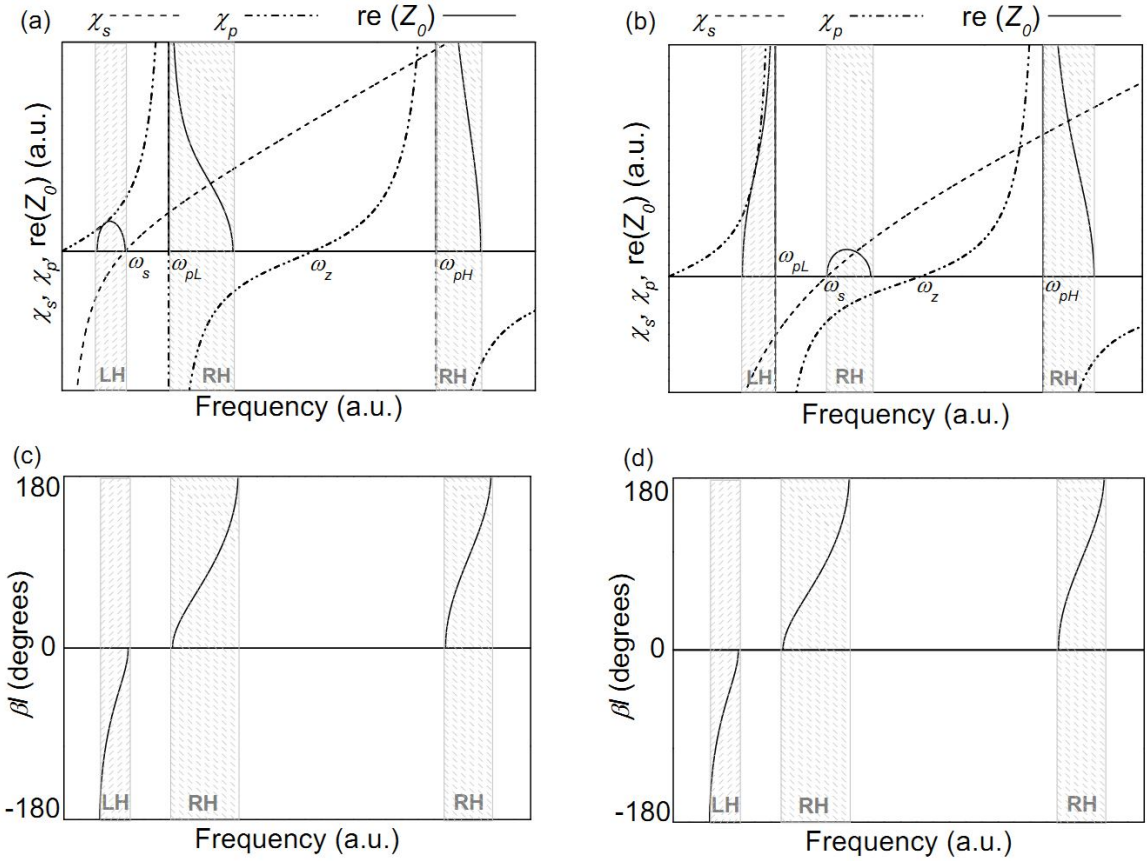

Figure 4.10: Representation of the series and shunt reactances, the characteristic impedance, and the phase (βl) for a unit cell as shown in figure 4.9(a). Two different cases have been considered: in (a) and (c) $\omega_s < \omega_{pL} < \omega_z < \omega_{pH}$, whereas in (b) and (d) $\omega_{pL} < \omega_s < \omega_z < \omega_{pH}$ [2].

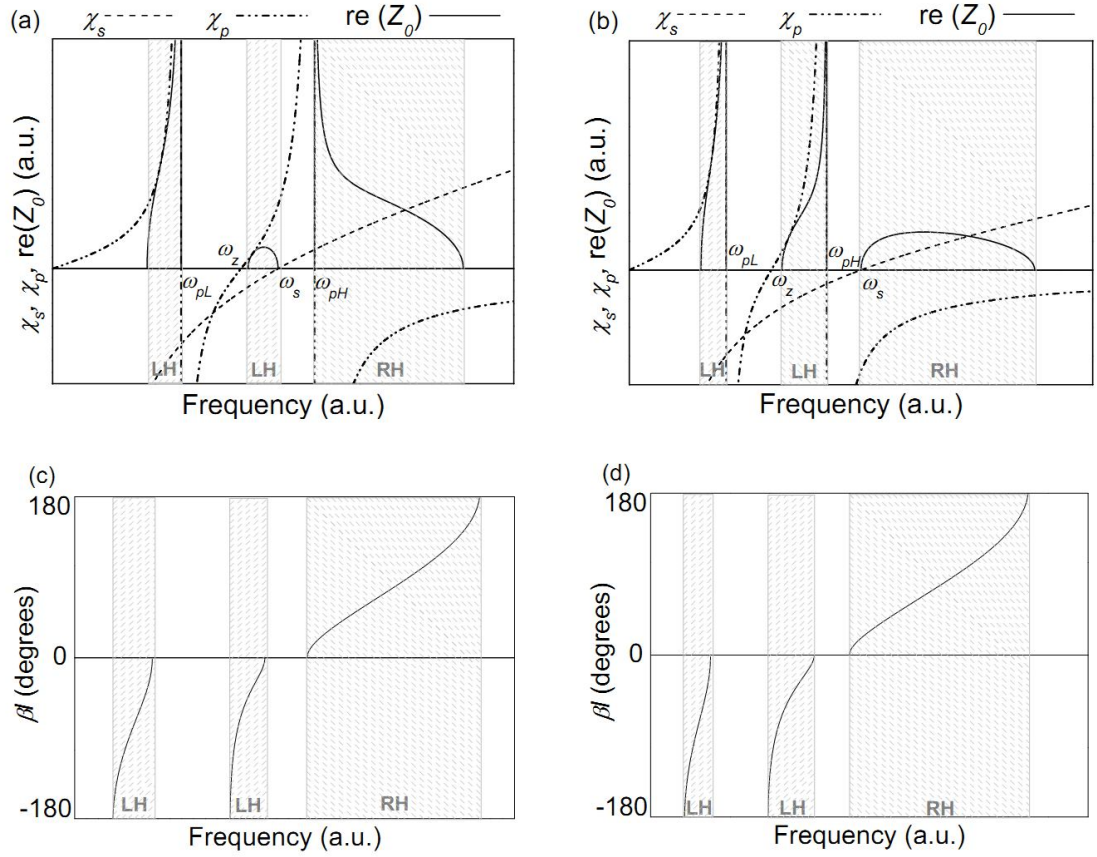

Figure 4.11: Representation of the series and shunt reactances, the characteristic impedance, and the phase (βl) for a unit cell as shown in figure 4.9(a). (a) and (c) $\omega_{pL} < \omega z < \omega s < \omega_{pH}$, whereas in (b) and (d) $\omega_{pL} < \omega_z < \omega_{pH} < \omega_s$ [2].

5- Resonant tunneling diode

5.1 Introduction

A resonant tunneling diode (RTD) is a diode with a resonant-tunneling structure in which electrons can tunnel through some resonant states at certain energy levels [4]. The resonant tunnel diode, also known as the Esaki diode, was first discovered by Leo Esaki in 1957 [4], when he discovered the field of internal emissions in heavily doped reverse biased germanium p-n junctions. He noted N-shaped current-voltage (IV) characteristic of this same junction when biased in the direction of forward bias similar to the I-V characteristic of the Si tunnel diode shown in Figure 5.1.

The tunnel diodes have more interesting features referring to the high switching speed and to the I-V characteristic that often exhibits negative differential resistance (NDR) regions. The current–voltage relationship of a tunneling diode is identified by the presence of one or more NDR regions, which enables many unique applications. It is used in wide range of applications such as an amplifier, pulse generators, ADCs and oscillators [4]. As well as incorporating tunnel diodes with transistors can improve circuit performance [17] by decreasing the power consumption or by increasing the speed of signal processing. On the other hand, the tunnel diodes are used in the manufacture of memory circuits where it can reduce static power dissipation relative to conventional approaches [4].

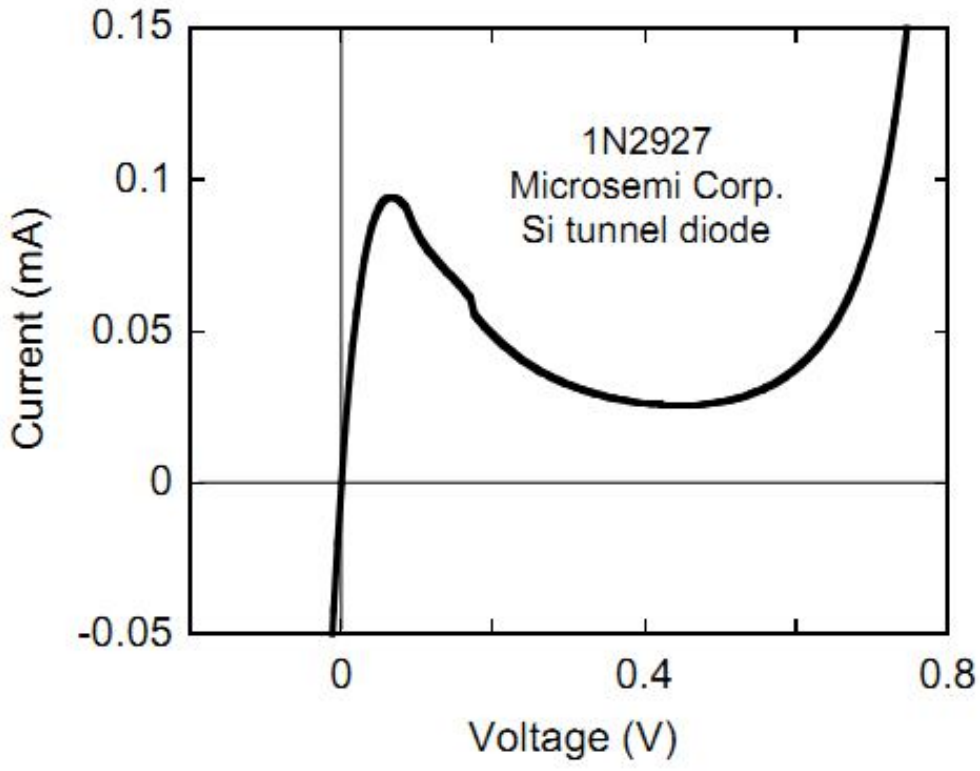

Figure 5.1: Current-voltage characteristic of a commercial silicon tunnel diode [4].

A new tunnel diode differential comparator has been proposed tunnel diode compared to the new differential which reduces the power dissipation by a factor of two relative to a transistor-only comparator with the increase in diode speed [18]. A particularly useful form of a tunneling diode is the Resonant Tunneling Diode (RTD) which can achieve a maximum frequency of up to 2.2 THz while the CMOS transistors can achieve a maximum frequency of up to 215 GHz [3].

Tunneling diodes provide the same functionality as a CMOS transistor where the device switching "on" when a specific external bias voltage range, biasing the device. In CMOS the current going through a channel between the drain and source while in RTDs the current goes through the depletion region by tunneling in normal tunneling diodes and through quasi-bound states within a double barrier structure in RTDs [3].

5.2 Theory of RTD Operation

Figure 5.2 shows the cross-section and corresponding conduction band diagram for the RTD. The cross-section of RTD consists of Four regions Emitter, Double-Barrier, Space-Charge, and Collector region [19]. The emitter region is a source of electron, and the Double-Barrier region consisting of two barriers and a quantum-well between these two barriers for large bandgap material, and the Space-Charge region is a drift region, while the Collector region is to collect the electrons tunneling through the double-barrier structure. The electrons from the emitter can tunnel to collector through the barriers if their longitudinal energy is equal to the energy of the quasi-bound state in the quantum-well.

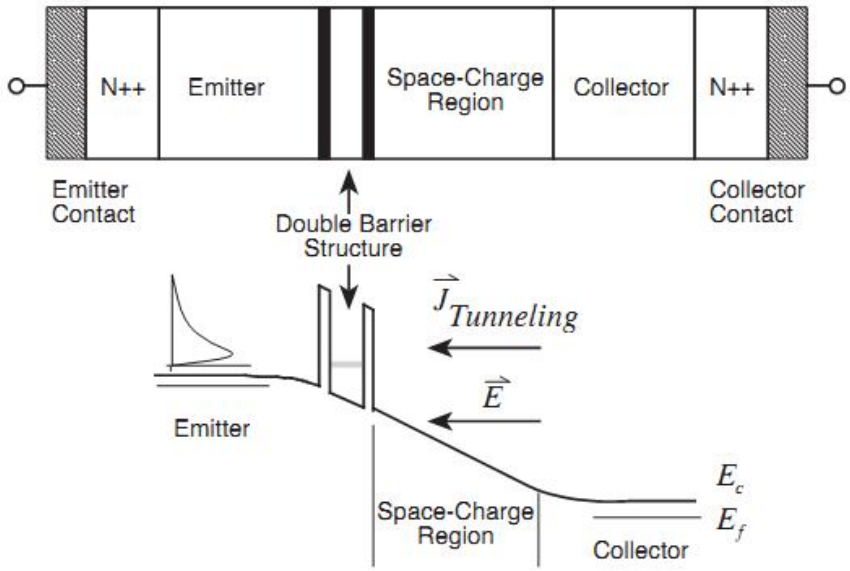

Figure 5.2: Cross-section of an RTD and the corresponding conduction band diagram under forward bias. The shaded region in the double-barrier structure represents the quasi-bound state in the quantum well. The energy distribution of the electrons in the emitter is also shown [19].

When Appling positive voltage at collector and negative voltage at emitter in the RTD (forward voltage), at near-zero electrical bias, the barriers region stop the electrons to flow from emitter, causing no current flow in RTD. Therefore, the electrons from the emitter form an accumulation layer near the barrier. When the forward voltage

increases, some of these electrons have an energy equal to the quasi-bound state energy in the quantum well which can tunnel through the double-barrier structure, giving rise to a current in RTD. With more increasing bias, the energy level of electrons in the emitter more than the energy level of the quasi-bound state in the quantum well, cause a great number of electrons tunneling, giving rise to an increasing current with applied voltage. The voltage and current are proportional to the current increase until the energy level of the quasi-bound state coincides with the energy level at which the peak in the emitter electron distribution occurs, this point of voltage called peak point (V_P) as shown in figure 5.3. After this voltage, the voltage and current are inversely proportional; the current decreases for increasing voltage which known with NDR. Beyond a certain applied voltage (valley) (V_V) the current then begins to rise with increased applied voltage.

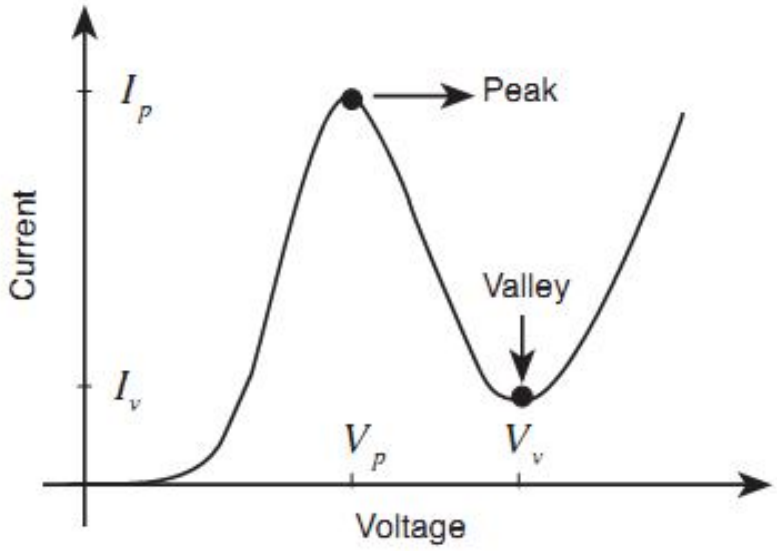

Figure 5.3: I-V characteristics of an RTD. The peak current (I_p) occurs at the peak voltage (V_p) and the valley current (I_v) occurs at the valley voltage (V_v) [19].

The applications of RTD are primary important on the NDR characteristics. The NDR characteristics are of primary importance for various RTD applications. Where the characteristics of NDR depends on two factor ; the peak current and peak voltage (I_p, V_p), and the valley current and valley voltage (I_v, V_v). There are other definitions which describe the NDR region; the current peak to valley ratio (PVR = I_p/I_v)), and negative conductance ($G_n = |\partial I/\partial V|$), where the G_n equal to the absolute value of the slope of I-V carve.

To design a specific NDR region parameters for a specific application, you need to justify the design of most components of RTD (quantum-well, barriers, emitter and space charge layers). For high frequency applications, we need very high peak current densities [19]. Where this can achieved by two ways, Reducing the thicknesses of the barriers or by increase the emitter doping level. Another example of the design of NDR region is the peak voltage (V_p) is determined by the thickness of the space-charge region and the quasi-bound state energy level.

5.3 Characteristic Model Equation

There are many models proposed to represent RTD I-V characteristic. The most famous models are stated below. The first method is to represent I-V characteristic by using the physics based models [20]. The major problem in all physics based models is that such models are usually complicated.

Shahhoseini *et al.* [21] obtained an analytical expression for I-V characteristic of Resonance Tunneling Diodes. This expression is based on quantum tunneling and includes physical parameters. Assuming Lorentzian approximation for transmission coefficient, they have offered Resonance Tunneling Diodes I-V equation by using quantum models as follows

$$f(V) = A \ln\left[\frac{1+e^{q(B-C+n_1V(t))/K_BT}}{1+e^{q(B-C-n_1V(t))/K_BT}}\right] .\left[\frac{\pi}{2}+\tan^{-1}\left(\frac{C-n_1V(t)}{D}\right)\right] + H\left(e^{n_2qV(t)/K_BT}-1\right) \quad (5.1)$$

In which $f(V)$ and V are current density and voltage, respectively. K_B, T, and q are Boltzmann constant, temperature in Kelvin and electron charge, respectively. A, B, C, and D are the dependent parameters on the device's physics which are obtained as follows:

$$A = \frac{em^*KT\Gamma}{4\pi^2h^3}, \quad (5.2)$$

$$B = \frac{E_F}{e}, \quad (5.3)$$

$$C = \frac{E_r}{e}, \quad (5.4)$$

$$D = \frac{\Gamma}{2e}, \quad (5.5)$$

where Γ, E_r, E_F, m^* and h are resonance width, the energy of wells resonance level, the energy of Fermi level, the effective mass and the reduced constant Plank, respectively. H, n_1 and n_2 parameters cannot be obtained easily from analytical method and are basically obtained by fitting.

The second method is to use a piecewise linear model [20]. This model depends on representing the I-V characteristic by three straight lines for three regions: positive differential region 1 (PDR1), the region of NDR and the positive differential region 2 (PDR2). It is clear that this model is simple and suitable for the simulation of spices, but it is not accurate, so it may give unrealistic results.

The third method is to use the Gaussian model-Exponential (G-E), Gaussian model uses exponential Gaussian curve to represent the tunnel current, and the exponential curve for the diode current normal [20]. This method has many advantages,

as it offers a compromise between simplicity and accuracy. It represents the full I-V characteristic by simple smooth curve that can reduce problems of convergence. The disadvantage of the GE model is that we can't control PDR1 and NDR separately, because it is similar to both with the same Gaussian curve.

The forth method, proposed in [22], is a modification of the G-E model. This model can control PDR1 and NDR regions separately. Consequently this model solved the disadvantage of G-E model. The disadvantage of this model is that it is complicated and the parameters extraction is not easy.

6- Literature Review

6.1 Introduction

In the last few years, an increased interest appeared in the scientific community for the study of metamaterial. Where the concept of the composite right/left-handed TL (CRLH-TL) was developed, and a number of novel applications have been demonstrated. Most researches of CRLH-TL consternate on linearity behavior of the TL depending on studying the shape and size of metamaterial cell especially on CSRR. Few of those researches presented the behavior of adding nonlinearity components to CRLH-TL such as adding Varactors diode to SRR cell. In other hand there are lots of researches talk about conventional nonlinearly TL such as adding RTD, varactors diodes and MOSFET to the TL. It is used in a wide range of application such as amplifier, pulse generators, analog-to-digital converters (ADCs) and oscillators [4].

In this chapter we present some of latest researches that related to our research. The previous studies divided to three sections CLRH-TL, nonlinear TL and nonlinear CRLH-TL. The CLRH-TL researches show the latest research about metamaterial behavior with different shape of cell. Nonlinear TL shows the effect of adding RTD to the right hand TL. While the nonlinear CRLH-TL show the application of adding Varactors diode and RTD to CRLH-TL.

6.2 CLRH-TL Previous studies

Atsushi *et al.* [23] presented characteristics of the CRLH-TL. Where the dispersion diagram of the two-dimensional CRLH-TL (figure 6.1) is obtained analytically based on the Bloch-Floquet theory, and the unique phenomenon of infinite guided-wavelength propagation, with nonzero group velocity at a nonzero frequency, is explained. They show analytically that when the CRLH TL is "balanced," two eigenfrequencies at the Γ point (phase constant = 0) of the Brillouin zone (BZ) degenerate at ω_{Γ} and a seamless transition from the LH to the RH modes without a bandgap can be achieved. Where Γ point eigenfrequencies $\omega_{\Gamma 1}$ and $\omega_{\Gamma 2}$ which delimit the upper and lower edges of the bandgap, are given by

$$\omega_{\Gamma 1}, \omega_{\Gamma 2} = \frac{1}{\sqrt{L_R C_L}}, \frac{1}{\sqrt{L_L C_R}} \tag{6.1}$$

(L_R, C_R) and (L_L, C_L) are inductance and capacitance of the TL in right and left handed respectively. The balanced case occurs at.

$$\frac{L_L}{C_L} = \frac{L_R}{C_R} \tag{6.2}$$

Kozyrev and van der Weide [24] proposed Nonlinear wave propagation phenomena in CRLH-TL media and simulates harmonic generation and parametric generation in a material that, in two dimensions. They discussed physical phenomena that lead to and affect self-supporting harmonic generation and parametric generation in LH nonlinear TL (NLTL) media and outline advantages of these media for developing new types of compact and efficient frequency multipliers and "active lens" devices.

Simulation of the LH NLTLs modeling is shown in figure 6.2 which demonstrates efficient harmonic generation. Harmonic generation is possible over a significantly wider operating frequency range and at relatively higher frequencies in comparison with the dual conventional low-pass filter NLTL. Furthermore, LH NLTLs are predicted to have advantages from the design perspective since they have more freedom to optimize parameters, being much less restricted by the host waveguide structure than in the case of RH periodically loaded NLTLs. Extending these results for 1-D LH NLTL to higher dimensions would enable combining harmonic generation in LH NLTL media with focusing, due to the negative refractive index of 2-D or 3-D LH transmission-line media.

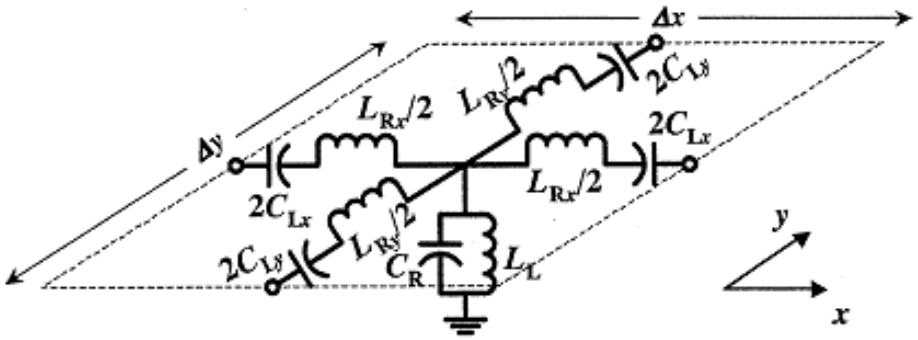

Figure 6.1: Unit cell of the 2-D CRLH TL [23].

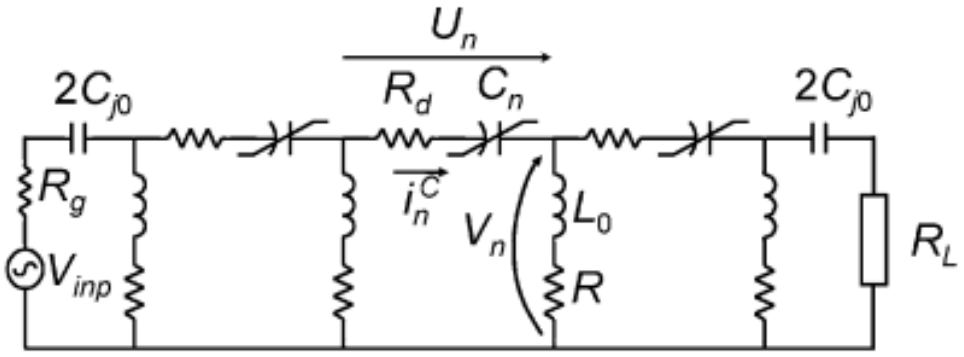

Figure 6.2: LH NLTL equivalent circuit [24].

Julien and Anja [25] proposed a CRLH TL Metamaterial Phase Shifters (MPS) in monolithic microwave integrated circuit (MMIC) Technology. Modeling and design of one-dimensional MPSs in monolithic microwave integrated circuit technology based on the CRLH-TL approach. From a theoretical point-of-view, they show that existing design expressions are restricted to phase shifters behaving as effective media, which is the case only if sufficiently large *L* and *C* loading elements can be designed in the given technology and at the frequency of interest. Therefore, they propose new design as shown in figure 6.3, which are exact on the basis of the circuit model of a unit cell in the structure. They show that the new expressions must be used to design integrated MPSs and the theory is verified by means of measurements of one and two cell phase shifters exhibiting a 0 phase shift at 17.5 GHz. The designed one cell phase shifter provides a

10-dB input return loss bandwidth larger than 10% with phase shifts of 29 and 30 at 16.5 and 18.5 GHz, respectively. The insertion loss is 1.3 dB at the center frequency and 1.7 dB at the limits of the bandwidth.

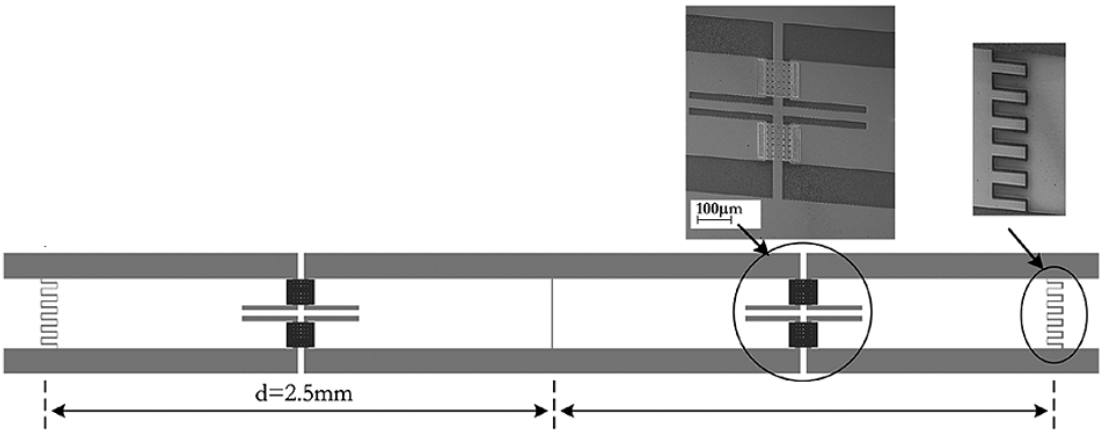

Figure 6.3: Right/left handed material as MPS [25].

Marta *et al*. [15] discussed in detail the transmission characteristics of CRLH TLs based on CSRR specifically, the necessary conditions to obtain a continuous transition between the left and right handed bands (balanced case). They designed two practical implications for the design of wideband and ultra-wideband (UWB) pass filters based on metamaterial transmission. One of them is based on the hybrid approach as shown in figure 6.4, where a microstrip line is loaded with CSRRs, series gaps, and grounded stubs; the other one is a bandpass filter, as show in figure 6.5, also based on a balanced line, but in this case, by using only CSRR and series gaps (purely resonant-type approach). These filters have very small dimensions (<1cm^2).

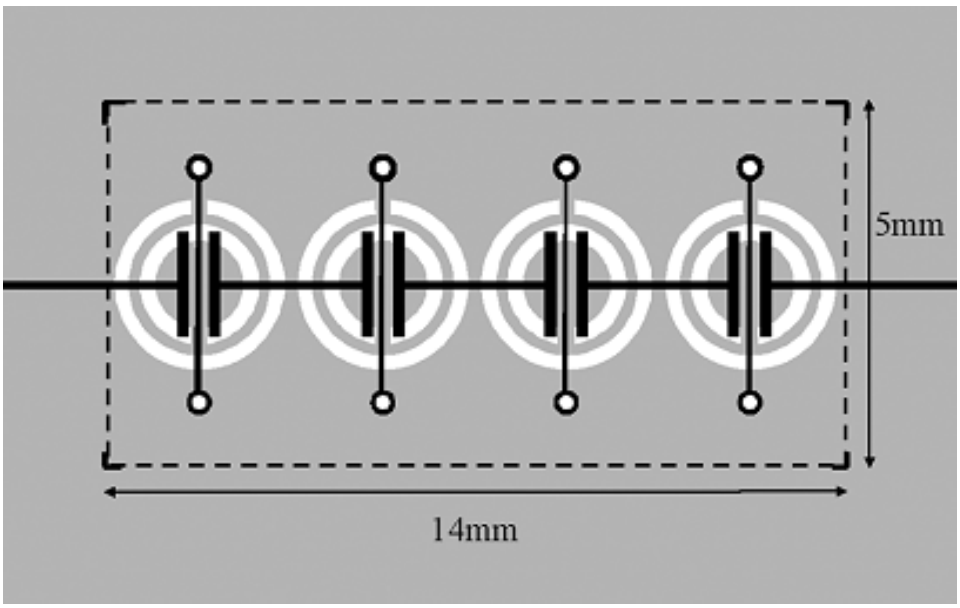

Figure 6.4: CRLH-TL based on the hybrid approach [15].

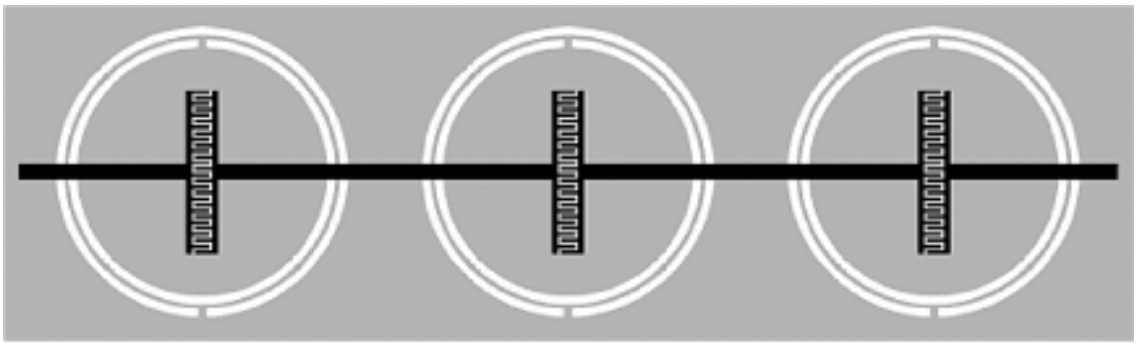

Figure 6.5: CRLH-TL based on purely resonant-type approach [15].

6.3 Nonlinear TL Previous studies

Slight *et al.* [26] Proposed an optoelectronic integrated circuit based on a resonant tunneling diode driving an optical communications laser diode as shown in figure 6.6 to operating as an optoelectronic VCO. Where this circuit can act as a VCO with optical and electrical outputs. They are restricted to relatively low frequencies (<10 GHz) on the oscillators. They show that the oscillator operation can be described by Liénard's equation and a second order nonlinear differential equation.

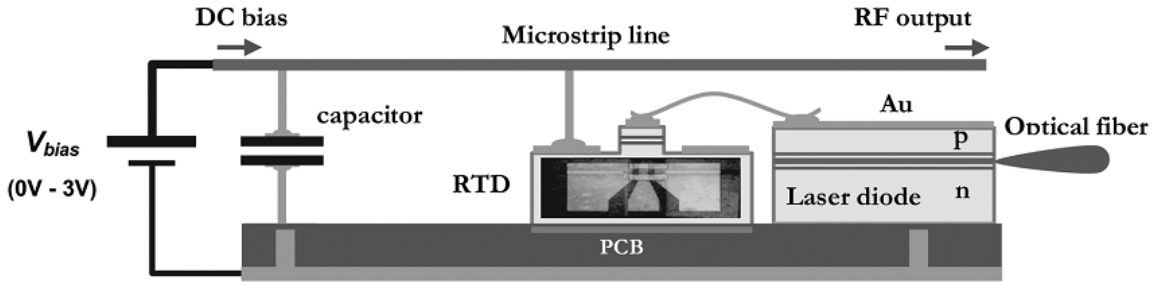

Figure 6.6: Representation of the electrical connections of RTD on the PCB [26].

Abu Ireban [27] proposed TLs and Schottky Diode to reshape incoming signal. Nonlinear relation between current and voltage for schottky RTD is introduced to obtain a general form of equation similar to Van Der Pol equation for an oscillator. Thus a signal reshaping and oscillator are designed by improving the TL characteristic by loaded Schottky Diode.

Yongsik *et al*. [18] proposed a RTD microwave oscillator operating at extremely low dc-power consumption. Which utilizes the antiphase-coupled quantum-effect RTD oscillations for efficient ac-power generation at a summing node of output based on a push–push principle. They fabricated the integrated circuit of the RTD microwave oscillator by using an InP-based RTD/HBT quantum-effect IC technology to show an extremely low total dc-power consumption of 85 μW at an oscillation frequency of 29.1 GHz when applied bias of 0.49 V. The device size of RTD is 0.7 ×0.7 μm2 as shown in figure 6.7.

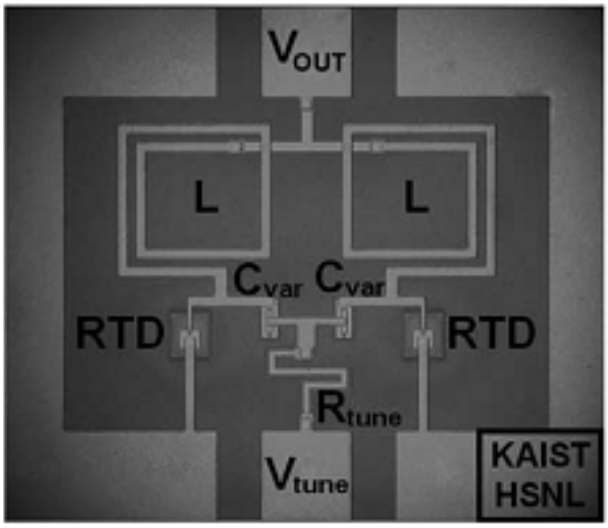

Figure 6.7: Microphotograph of the fabricated RTD oscillator [18].

AL-Farra *et al*. [28] proposed a new design of nonlinear transmission, which is loaded with RTD to be suitable for microwave ADC. Where the RTD-NLTL is a coplanar transmission line periodically loaded with RTDs. Figure 6.8 shows the equivalent circuit of the nth section of the RTD-NLTL.

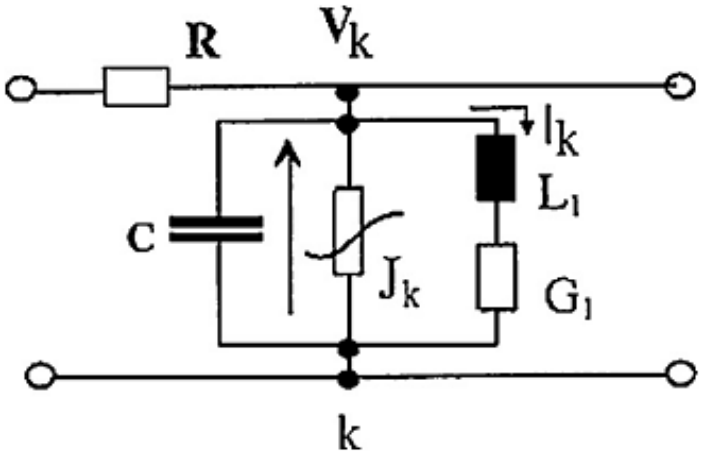

Figure 6.8: Schematic representation of the nth section of RTD-NLTL [28].

6.4 Nonlinear CRLH-TL Previous studies

Kuylenstierna *et al*. [29] proposed CRLH-TL phase shifter, using ferroelectric varactors as tunable element. They demonstrated theoretically and experimentally how the unique features of CRLH-TLs enables a differential phase shift with flat frequency dependence around the center frequency. The experimental prototype is a coplanar includes four CRLH T-unit cells and has a physical length of 3.850 mm as shown in figure 6.9. The ferroelectric varactors are realized in parallel plate version. Under 15-V dc bias applied over each varactor, the differential phase shift is flat around 17 GHz.

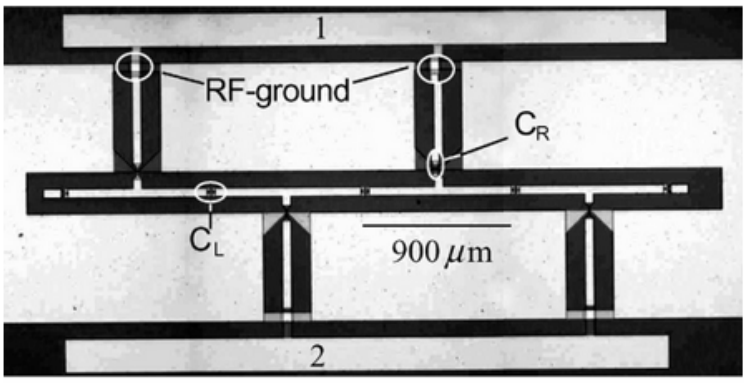

Figure 6.9: CRLH phase shifter [29].

Jaewon *et al*. [30] proposed a broadband VCO using tunable metamaterial TL with varactor-loaded SRR (VLSRR) as shown in figure 6.10. They demonstrated that VLSRR coupled to microstrip line can lead to metamaterial TL with tuning capability. Where the negative effective permeability is provided by the VLSRR in a narrow band above the resonant frequency and the bias of VLSRR is controlled by the varactor diodes.

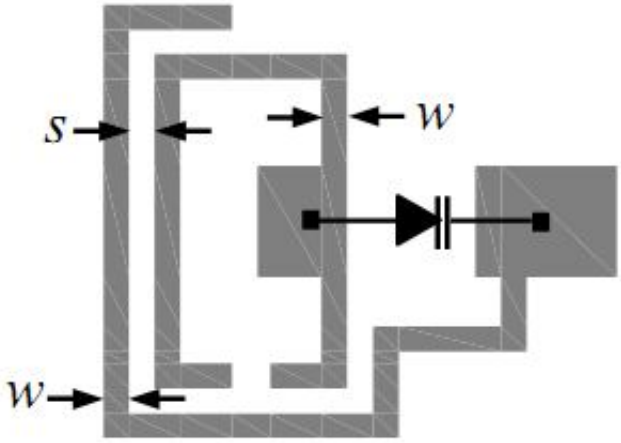

Figure 6.10: Tunable varactor-loaded SRR [30].

Maezawa *et al*. [31] proposed a traveling wave amplifier based on CRLH-TL periodically loaded with RTD pairs. They discussed stability of the TL loaded with RTDs, and showed that it can be stabilized by using CRLH TL configuration. They designed the circuit that consists of 160 unit cells where one cell is shown in figure 6.11 to obtain approximately 10 dB gain. It was demonstrated that this amplifier can have a gain for wide frequency range.

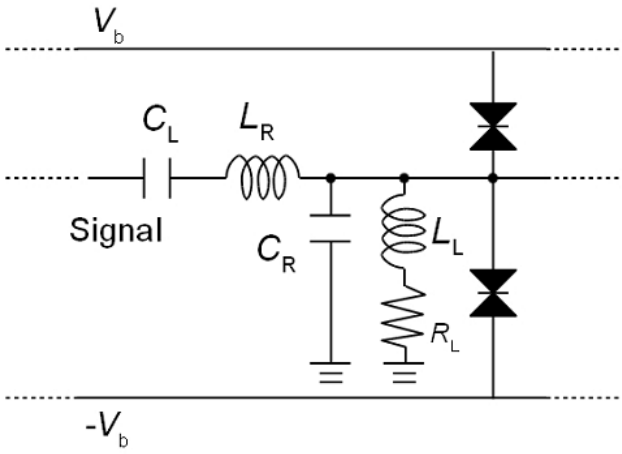

Figure 6.11: Unit cell of the CRLH-TLs periodically loaded with RTD pairs [31].

7- Nonlinear Composite Left/Right handed TL Media with RTD Application and Simulation

7.1 Introduction

The purpose of this work is to study the behavior of CLRH-TL with RTD. CRLH-TL based on the modified hybrid approach, where a microstrip line is loaded with CSRRs, series gaps, and shunt inductor. There are two goals of this work. The first goal is to design TL capable of filtering and amplifying the signal at very wide bands. The second goal is to design voltage control oscillator at high frequency.

7.2 First model: filter with amplification

Our model is an ultra-wideband filter with amplification at frequency range form 5-10.5 GHz. The filter is constructed by combining the RTD with CRLH-TL based on modified hybrid CSRR. The CRLH-TL which presents in [15] as shown in figure 6.4 consists of four cells and subjected to the following specifications: active area below 1 cm^2, bandwidth covering the 4–10 GHz and in-band ripple lower than 1 dB. Figure 6.4 shows the construction of these cells where the metallic parts are depicted in black in the top layer, and in gray in the bottom layer. The rings are etched on the bottom layer. The dimensions of the cells: line width W=0.126 mm, external radius of the outer rings r=1.68 mm, rings width c=0.32 mm and rings separation d=0.19 mm; inductor width is 0.10 mm and the distance between the metals forming the gap is 0.4 mm

The unit cell is designed with the series resonance frequency as close as possible to the higher resonance of the shunt impedance ($\omega_S = \omega_{PH}$). This gives a transmission zero below the passband of interest, which is useful to obtain high rejection below the required band. Although below that transmission zero there is a LH passband, it is very narrow for the designed structures and its effects are irrelevant [15]. The simulated frequency response of this unit cell is depicted in figure 7.1.

Above the passband of interest, which extends approximately from 3 to 10 GHz, there is an additional transmission zero (between 12 GHz–13 Hz), which is not explained by means of the equivalent circuit model of the hybrid CSRR (see figure 4.9(b)) for the situation that we are considering ($\omega_S = \omega_{PH}$). In addition, a transmission peak is also present at 13.7 GHz. This behavior can be explained by considering the effects of the second resonance frequency of the CSRR. This is explained by the fact that these particles exhibit several resonance frequencies [13], [32]. The first one, the quasi-static resonance, is the resonance of interest for most of the applications of CSRR. However, at higher frequencies, there are additional resonance frequencies (dynamic), which may play a role under certain circumstances. Namely, an additional parallel branch will added to the conventional model circuit (figure 4.9(b)) to account for the second resonance of the CSRR. Figure 7.2 shows the new equivalent circuit that includes the effects of the second resonance (new branch; C_2, C_{c2} and L_{c2}). Where the parameters of the new model: L = 2.6 nH, C_g = 0.2pF, L_d = 5.4 nH, C_1 = 305 pF, C_{C1} = 0.65pF, L_{C1} = 0.55nH, C_2 = 0.21pF, C_{C2} = 0.32 pF, and L_{C2} = 0.27 nH [15]. It is interesting to mention that the coupling capacitance of this new branch, i.e., C_{c2}, is very small. This is consistent with the fact that electric coupling is very weak at the second resonance of CSRR [13], [32]. The presence of the second resonance of the CSRR plays a fundamental role in order to obtain a sharp cutoff above the passband of interest, and

this is clear from the figure 7.1. The position of the two transmission zeros can be controlled with the dimensions of the CSRR and gaps.

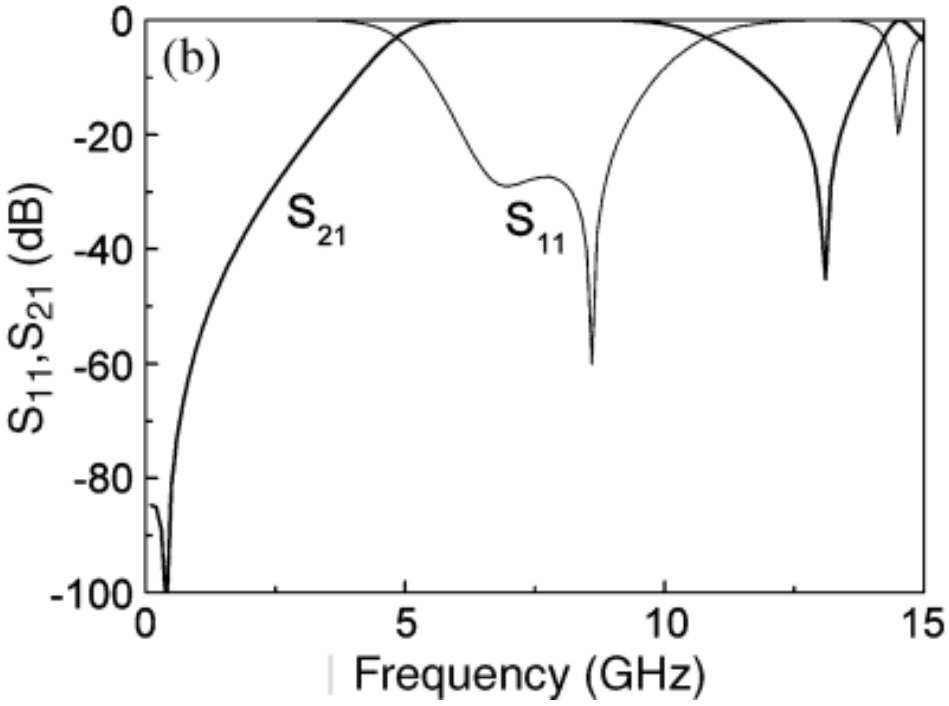

Figure 7.1: Simulated reflection and transmission coefficient of a single cell corresponding to the filter shown in figure 6.4 [15].

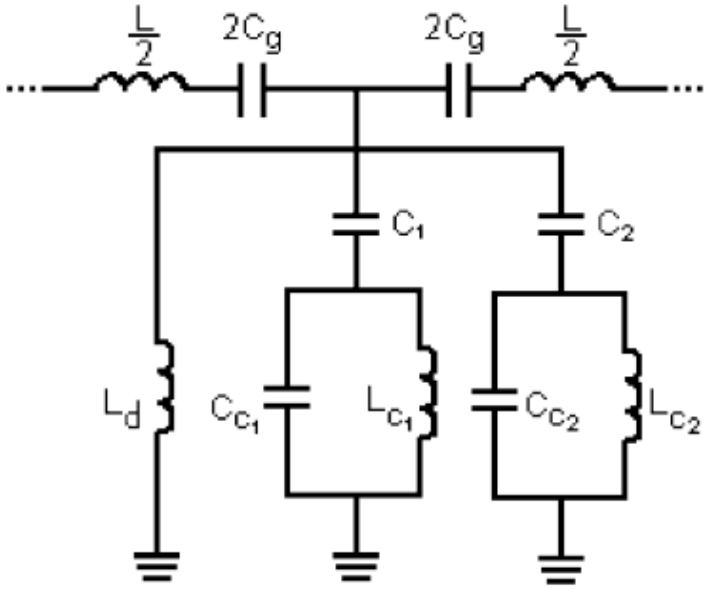

Figure 7.2: Equivalent circuits of one hybrid CRLH cells that shown in figure 6.4.

From the circuit model of figure 7.2, both transmission zeros are given by equation (4.52) by replacing C, L_C and C_C by the corresponding reactive elements (C_1, L_{C1} and C_{C1} for the lower transmission zero and C_2, L_{C2} and C_{C2} for the upper transmission zero).

$$F_{z1} = \frac{1}{\sqrt{L_{c1}(C_1 + C_{c1})}} = 388 \text{ MHz} \tag{7.1}$$

$$F_{z2} = \frac{1}{\sqrt{L_{c2}(C_2 + C_{c2})}} = 13.30 \text{ GHz} \tag{7.2}$$

Obviously, the small frequency value of the first transmission zero can be only explained by a large coupling capacitance C_1, which has been estimated to be in the vicinity of 300 pF. This capacitance is much larger than the coupling capacitance corresponding to the second resonance, as expected since the electric excitation of the second resonance is very weak.

The series Z_S for the model circuits (figure 7.2) remains the same as in equation (4.48) while shunt impedances Z_P, characteristic impedance Z_o and phase shift per cell $\Phi = \beta l$ are changing according to the new branch (C_2, L_{C2} and C_{C2}).

$$Z_p = j\alpha^{-1} \tag{7.3}$$

$$\alpha = \frac{1}{\omega L_d} + \frac{\omega C_1\left(\omega^2 C_{c1} L_{c1} - 1\right)}{1 - \omega^2 L_{c1}(C_1 + C_{c1})} + \frac{\omega C_2\left(\omega^2 C_{c2} L_{c2} - 1\right)}{1 - \omega^2 L_{c2}(C_2 + C_{c2})} \tag{7.4}$$

$$Z_0 = \sqrt{\frac{\left(1 - \omega^2 C_g L\right)}{\omega 2 C_g}\left[2\alpha^{-1} - \frac{\left(1 - \omega^2 C_g L\right)}{\omega 2 C_g}\right]} \tag{7.5}$$

$$\cos \beta l = 1 - \frac{\left(1 - \omega^2 C_g L\right)}{\omega 2 C_g}\alpha \tag{7.4}$$

There are three shunt resonance frequencies that null the corresponding admittance, two of them are the lower and higher resonance frequencies (ω_{PL}, ω_{PH}) of the hybrid approach CSSR and the third resonances frequencies correspond to new shunt branch. Figure 7.3(a, b) show the series and shunt reactance of the unit cell that shown in figure 7.2 for low and high frequency range. From figure 7.3(a, b) we notice that the lower and higher shunt resonance frequency equal to 0.118 GHz and 7.51 GHz respectively, while the resonance frequency ω_S equal to 6.917 GHz. This implies that ω_{PH} in near to ω_S and not exactly balanced.

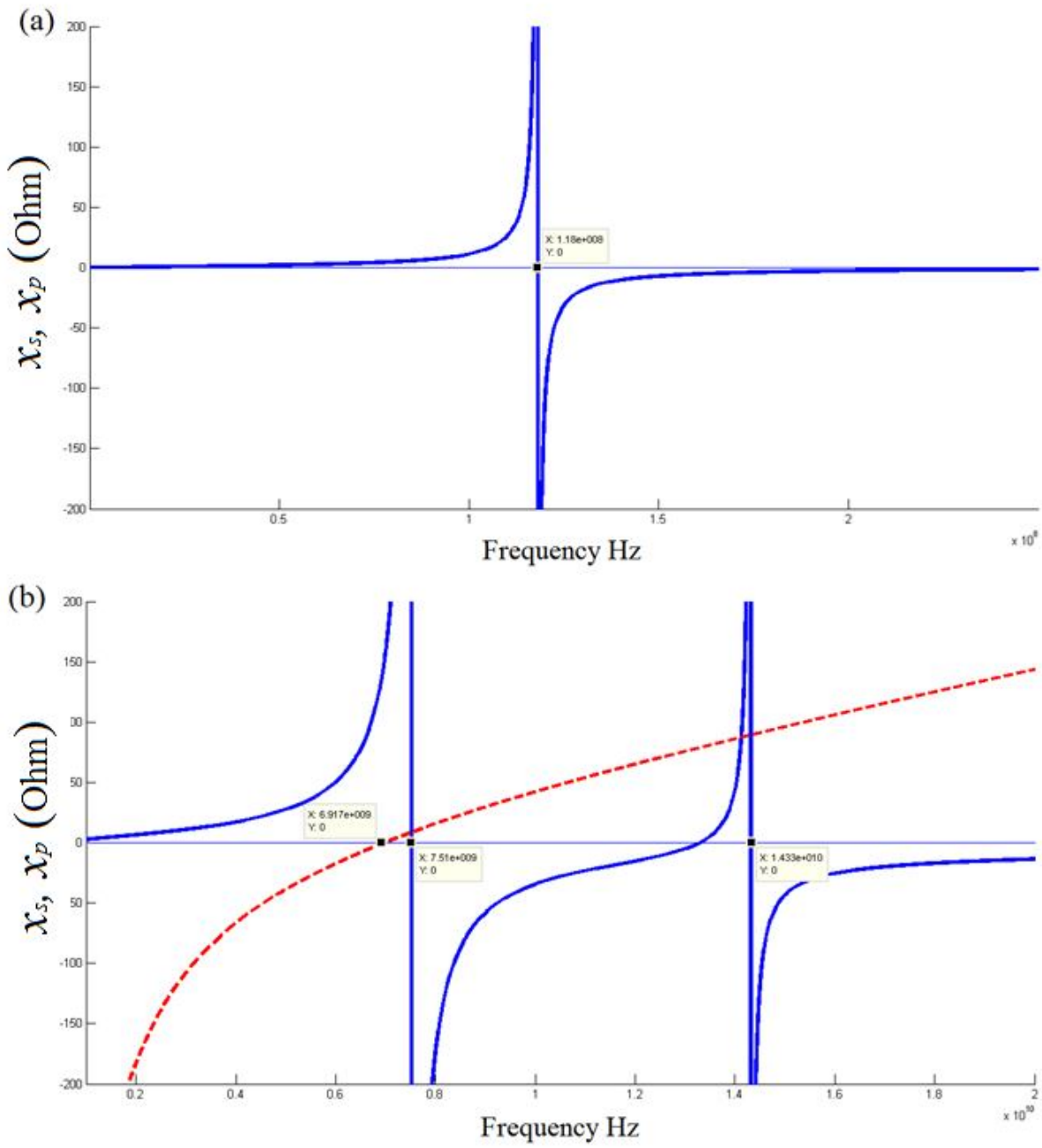

Figure 7.3: Dependence of series and shunt reactance of the unit cell shown in figure 7.2 on frequency drown by MATLAB. Dash line refers to the series reactance and the solid line refers to the shunt reactance. (a) frequency range varies between 1-250 MHz. (b) frequency range changes between 0.5-20 GHz.

7.2.1 Modified hybrid model

Up to this moment, we only do an analysis of the CLRH metamaterial cell in [15]. Now, we will study the effect of adding RTD to the previous cell. The objective of our study to make UWB filter with amplification. We put the RTD and DC voltage source at shunt with grounded stubs of CRLH-TL cell (figure 7.4) and tune the DC voltage source until achieve the desired design. The equivalent circuit model of one cell

with RTD is shown in figure 7.5 where the equivalent RTD model and DC biasing source is shunt with inductance L_d [2].

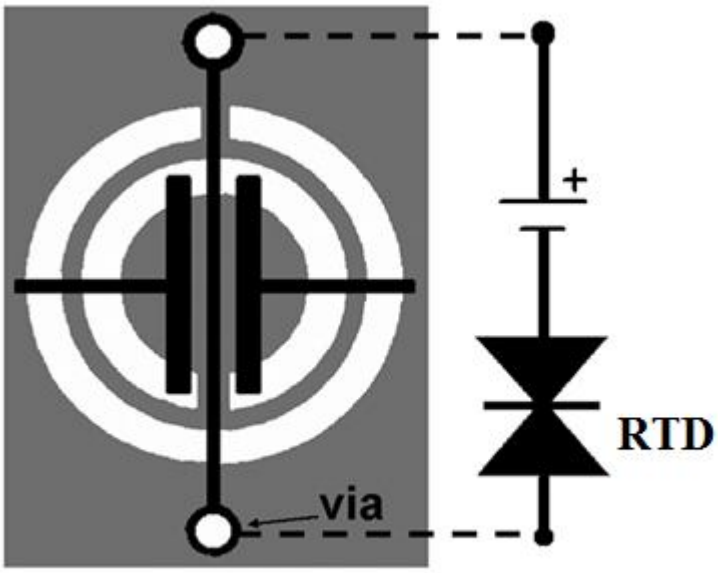

Figure 7.4: RTD at shunt with grounded stubs of the hybrid CRLH cells.

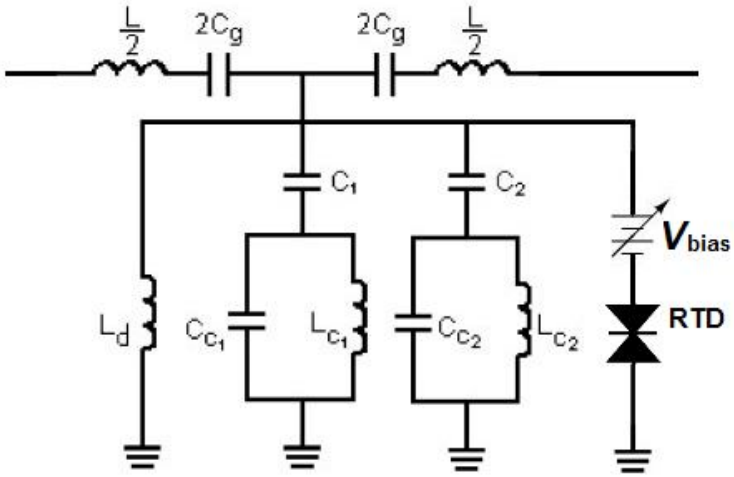

Figure 7.5: Equivalent circuit model of the unit cell (figure 7.2) with RTD shunt with grounded stubs.

The experimental RTD I_V characteristic is fitted using the physics based description of the RTD equation (5.1). Figure 7.6 displays the current ($I=f(V)$) as function of V using the fitting parameters from [26], A = 6.48x10^{-3}, B = 0.0875, C = 0.1449, D = 0.02132, H = 7.901x10^{-4}, n_1 = 0.1902, n_2 = 0.0284, and T = 300 K.

From the figure 7.6 we note the peak current and voltage on the RTD (I_p, V_p) equal (41 mA, 0.675 V) respectively, and the valley current and voltage of RTD (I_v, V_v) equal (11 mA, 1. 481 V) respectively, this meaning that the NDR region lies form 0.675 V to 1.481 V. where The NDR characteristics are primary important for our applications.

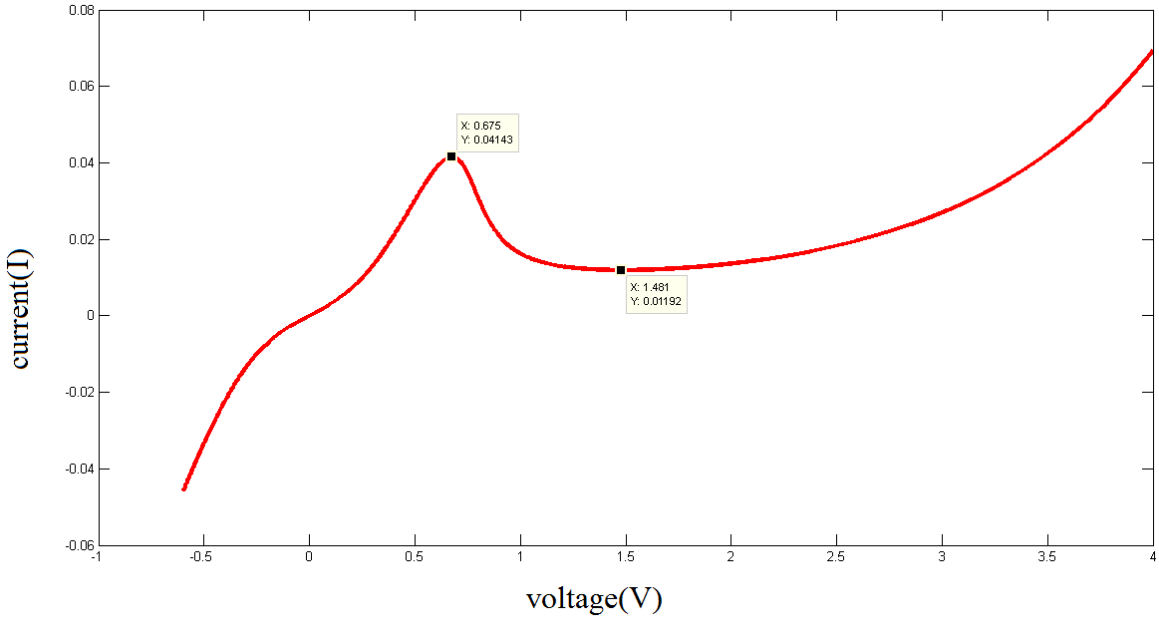

Figure 7.6: I-V characteristics of the RTD in our simulation.

The RTD was biased using a series variable DC voltage supply producing amplification when biased in the NDR region. Figure 7.7 shows the Simulated reflection and transmission coefficient (through Agilent ADS) of a single cell with RTD, corresponding to the filter shown in figure 7.5 at different DC biasing changes form 1.16 to 1.38 by increment of 0.2V referring to figure 7.7(A-L) respectively, where dash line refers to S_{21} and the solid line refers to the S_{11}. From figure 7.7, we see the effect of RTD on the transmission coefficient, the value of S_{21} is more than 0 dB compared to the value of S_{21} on the original cell (maximum value is 0 dB as shown in figure 7.1). This indicates that the output power of the filter is bigger than the input power. The value of S_{21} depending on the value of DC biasing.

The filter simulated results for equivalent circuit (figure 7.5) is shown in figure 7.8. It is shown in figure 7.8 the transient response at different input frequency signal range between from 5-10 GHz with DC biasing 1.18 V and the peak value of input signal equals 50 mV. It is clear that the amplification of the input signal occurs at range of frequencies from 5-10 GHz and the value of amplification depends on the input frequency i.e. the peak value increases from that 50 mV to 75 mV at frequency 9 GHz with amplified value equals 50 percent.

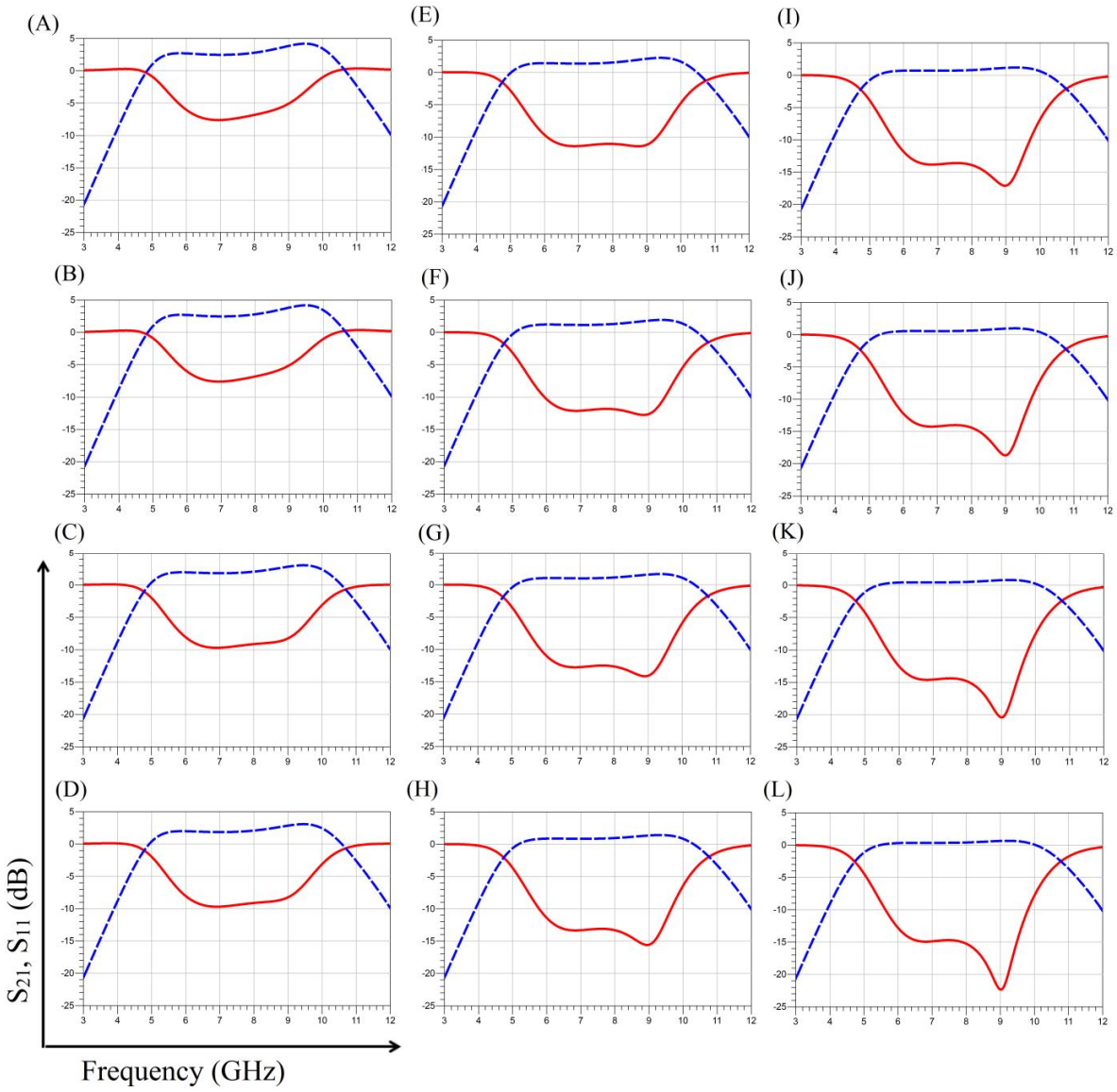

Figure 7.7: Simulated reflection and transmission coefficient of a single cell with RTD, corresponding to the filter shown in figure 7.5 at different DC biasing voltage. (A) V_{bias} = 1.16 V, (B) V_{bias} = 1.18 V, (C) V_{bias} = 1.2 V, (D) V_{bias} = 1.22 V, (E) V_{bias} = 1.24 V, (F) V_{bias} = 1.26 V, (G) V_{bias} = 1.28 V, (H) V_{bias} = 1.3 V, (I) V_{bias} = 1.32 V, (J) V_{bias} = 1.34 V, (K) V_{bias} = 1.36 V and (L) V_{bias} = 1.38 V. The dash line refers to S_{21} and the solid line refers to the S_{11}.

There are two cases of our filter with RTD that distort the input signal and change the shape of the input signal. The first case when the V_{bias} as near as to the V_p of RTD at NDR region that can be shown in figure 7.9 when V_{bias} equal to 0.9 V. We can show that the reflection and transmission coefficient is more than 0dB. In this case the filter works as a frequency oscillator that will be discussed later in this chapter. The second case of distorting input signal is occurs when the peak value on input signal is relatively large. Where the value of input voltage depends on the value of V_{bias}. In other words, when the input signal equal to 100 mV and V_{bias} equal to 1.18 V the input signal

is distorted as shown in figure 7.10. This case will discussed later as we discuss the reasons of amplification on our filter.

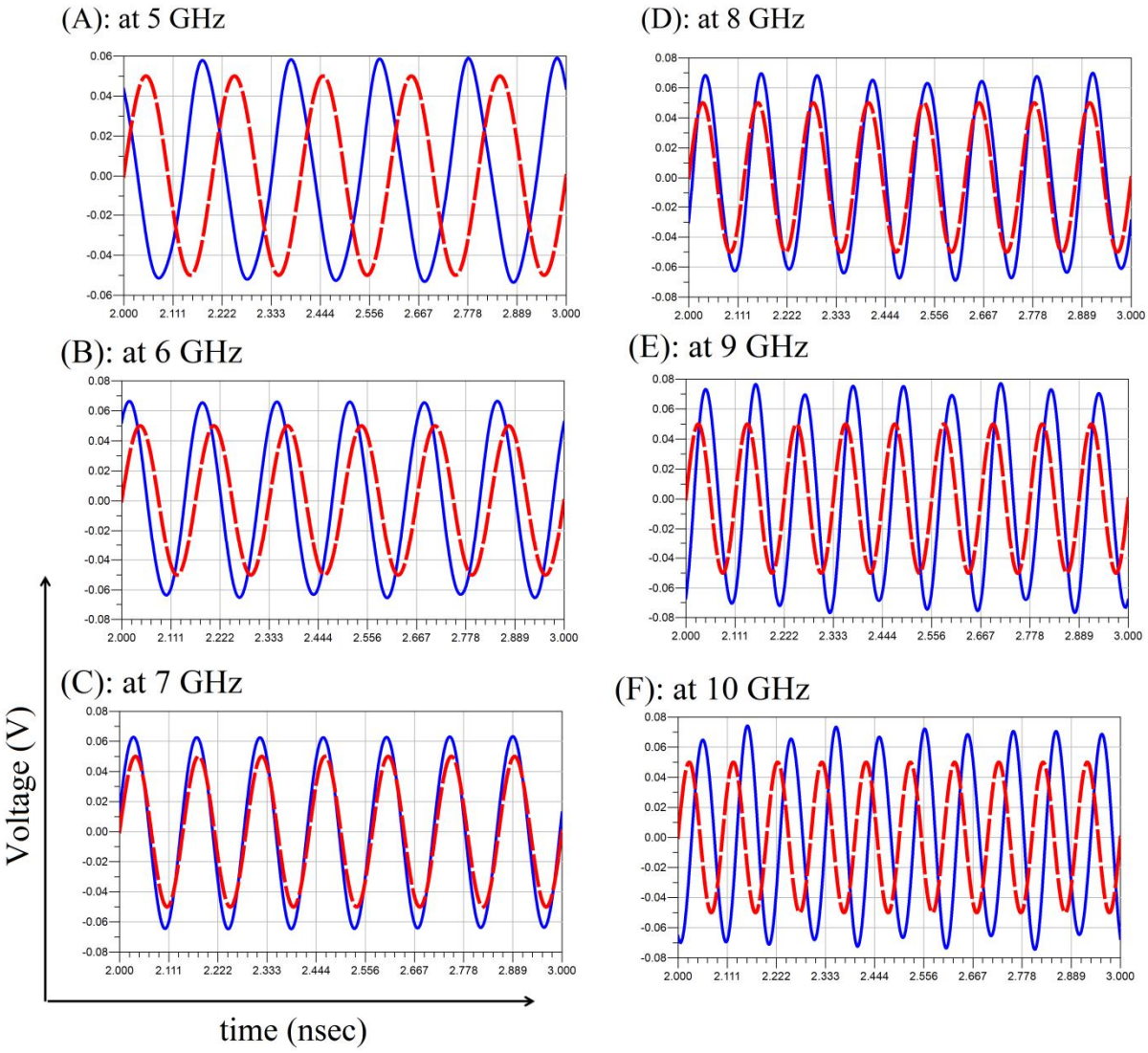

Figure 7.8: Simulation results to the Equivalent circuit shown in figure 7.3 at time domain when V_{bias} equal 1.18V at different input frequency. The input frequencies are indicated in the figures . The dash line refers to the input signal and the solid line refers to the output signal from the filter.

To understand the effect of RTD, we focused on the NDR region of RTD. Figure 7.11 displays RTD I_V characteristic extends from 1.1 to 1.3 V where this region is located in NDR. We notice that (figure 7.11) the relationship between voltage and currant is linear; therefore, we can replace the original equation of RTD by the approximated equation (7.5)

$$I = slope * V = A'V \tag{7.5}$$

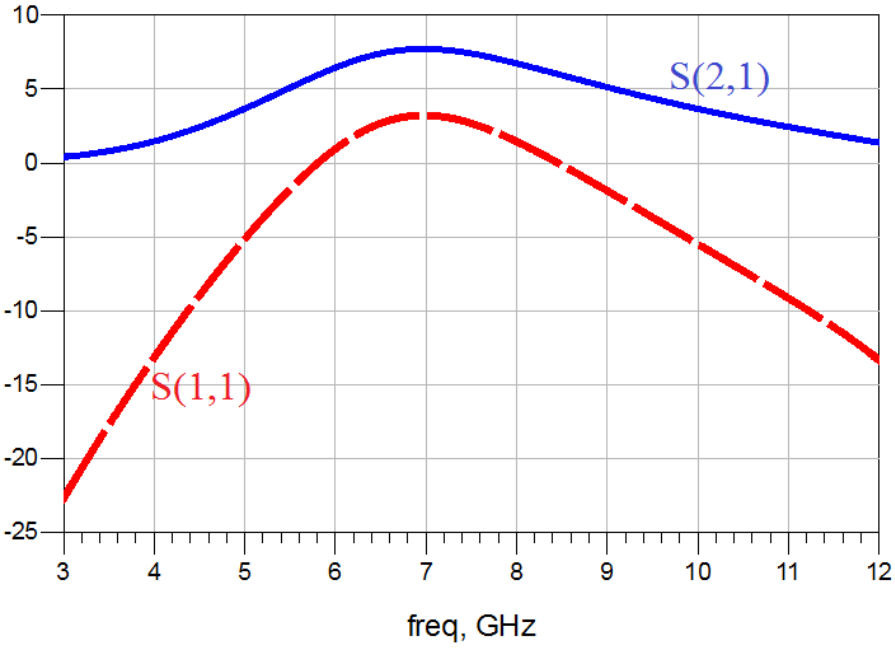

Figure 7.9: Simulated reflection and transmission coefficient of a single cell with RTD, corresponding to the filter shown in figure 7.5 at voltage DC bias 0.9V. The dash line refers to S_{21} and the solid line refers to the S_{11}.

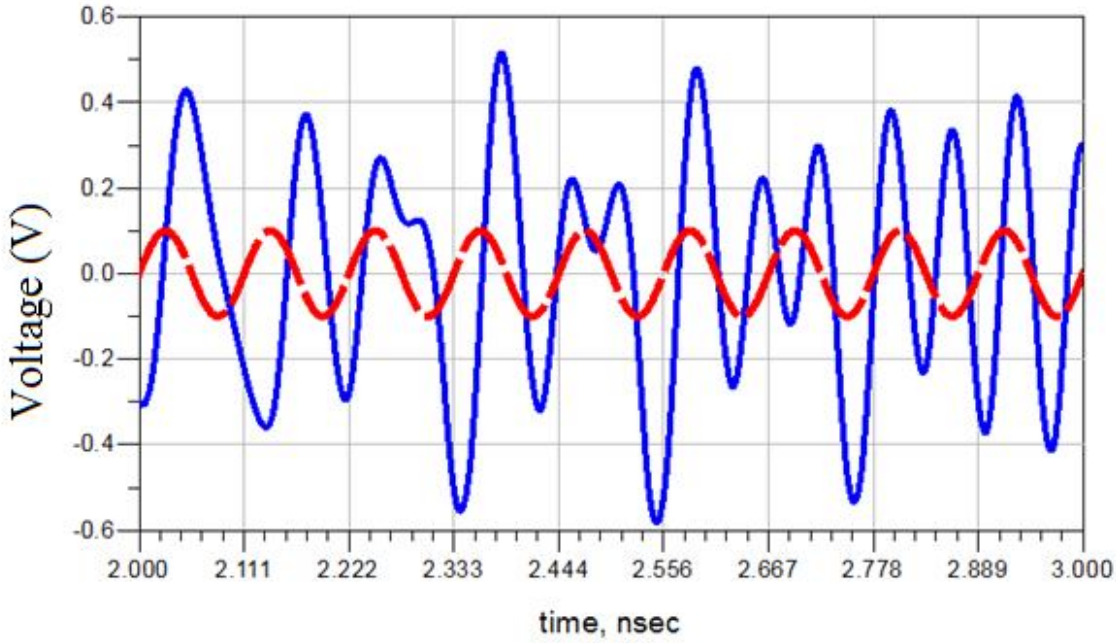

Figure 7.10. Simulation result to the equivalent circuit shown in figure 7.3 at time domain when input signal 100 mV peak value at 9 GHz and V_{bias} equal to 1.18V. The dash line refers to the input signal while the sold line refers to the output signal.

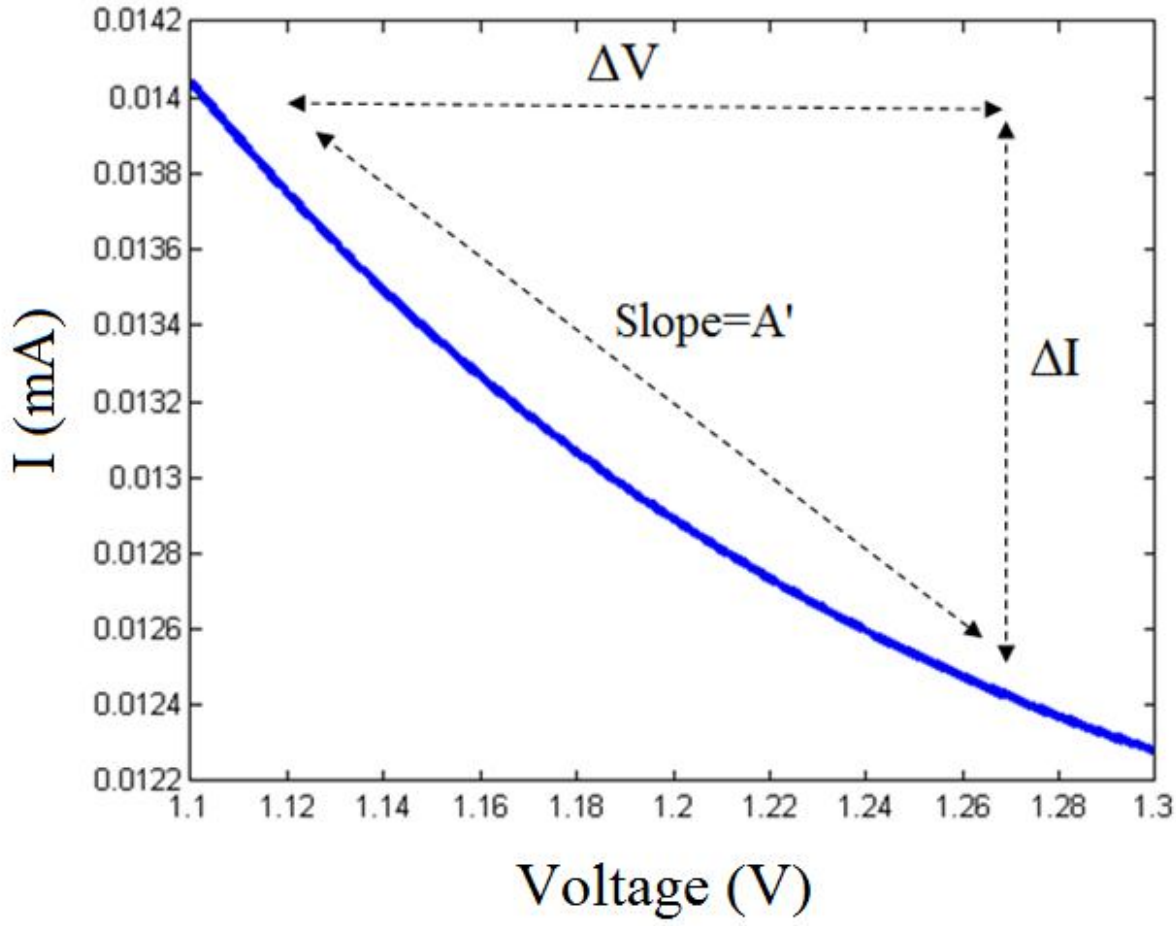

Figure 7.11: I-V characteristics of the RTD in the voltage range from 1.1 to 1.3 V.

Where the *A*' equals to the slope of currant at the working regain and *V* is the voltage drop at RTD terminal. The value of the slope depends on the V_{bias}. Figure 7.12 shows approximated equivalent circuit model of the unit cell (figure 6.4) with RTD replaced by variable current source equation (7.5). For proving the approximated equation of RTD, we replaced the RTD by a variable current source as a function of voltage *I=A'V* and compared the results with real RTD.

Form figure 7.11, at V_{bias} equal to 1.18, the slope of V_I approximately equals to -0.09. We simulated the circuit model (figure 7.12) with variable current source function of voltage (*I=-0.09V*) with exciting input signal 50 mV peak value and 9 GHz (figure 7.13). It is clear that the results are similar to one we obtain in figure 7.8(E) at 1.18 V_{bias}.

Now we can explain why the signal must be relatively small, because when the input signal is large the voltage drop at RTD terminal will extend in nonlinear region and the slope of V_I characteristics is not constant at all time of input signal.

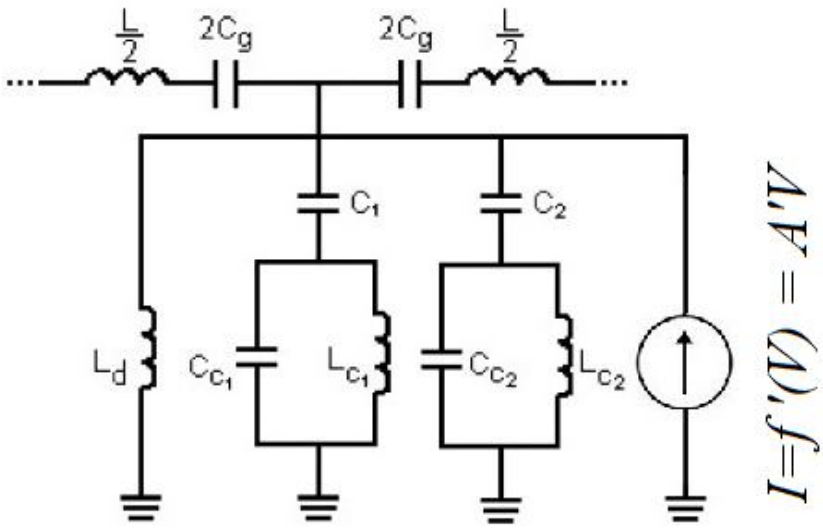

Figure 7.12: Equivalent circuit model of the unit cell (figure 6.4) with RTD replaced by variable current source *I*.

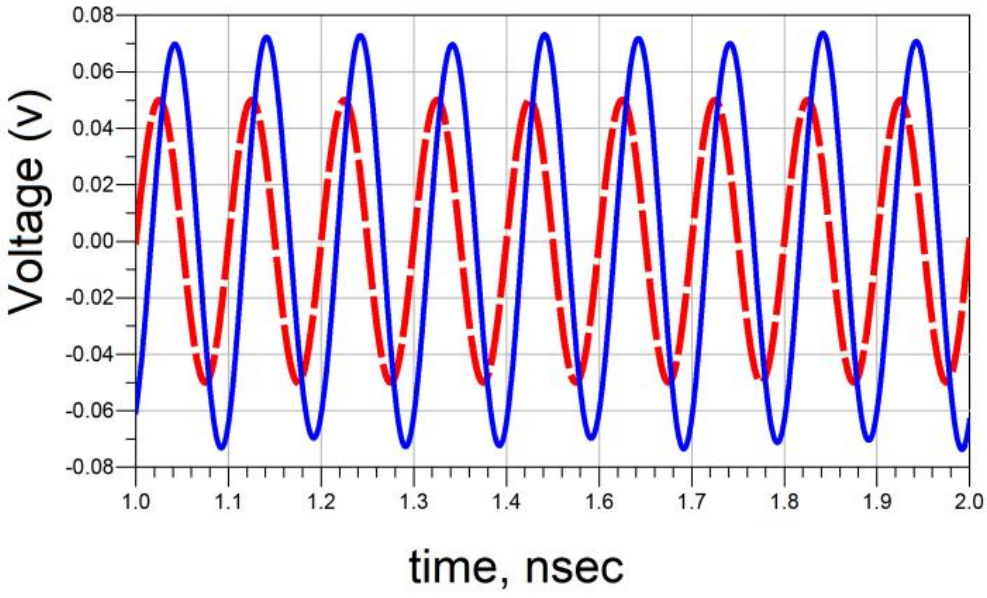

Figure 7.13: Simulation results of the equivalent circuit with approximated RTD equation shown in figure 7.12 in the time domain at 9 GHz where the dash line refers to the input signal and the solid line refers to the output signal of the filter.

7.2 Second model: voltage controlled oscillator

Our model is a VCO. The main goal of this model is to study left- and right-handed TL in CSRR with RTD to obtain VCO. The model is constructed by combining the RTD with CRLH-TL based on modified hybrid CSRR. The CRLH-TL as shown in Fig. 6.4 and RTD with V_I characteristic as shown in figure 7.6. We put the RTD and DC voltage source at shunt with grounded stubs of CRLH-TL cell and tune the DC voltage source until we achieve the desired design.

To illustrate the potentiality of CRLH-TL loaded with CSRR compound with RTD to the design VCO, three prototype device examples are provided. The first one is a one cell as shown in figure 7.4 with short circuit at the beginning of the cell between ground and patch, and 50 Ω load resistance at the end of the cell between ground and patch. The second one is similar to the first prototype but with open circuit at the beginning of the cell instated of short circuit. The third prototype consists of one cell as shown in figure 7.4 with two 50 Ω load resistances between ground and patch at both the beginning and at the end of the cell. The equivalent circuit model of the three prototypes (first, second and third) are shown in figure 7.14(a, b, c) respectively where the equivalent RTD model and DC biasing source is shunt with inductance L_d and R_L is the resistance of the load for output signal. The RTD was biased using a variable DC voltage supply producing voltage oscillator at resistance load when the RTD biased in the NDR region. The DC voltage source was put at series with RTD to shift the I_V characteristic to NDR.

Figure 7.15 shows the simulation output voltage in time and frequency domain at R_L for the first case model (figure 7.14(a)) at two different values of V_{bias}. Figure 7.15(a) shows the output voltage at R_L when V_{bias} equal to 0.7V and its frequency domain spectral shown in figure 7.15(b). While figure 7.15(c) shows the output voltage at R_L when V_{bias} equal to 1.1V and its frequency domain spectral shown at figure 7.15(d). From the frequency spectral is we noticed that there are three main frequencies 4.8, 9.7 and 14.6 GHz appeared when V_{bias} equal 0.7 and only 14.6 GHz appeared at 1.1 V_{bias}.

Figure 7.16 shows the simulation output voltage in time and frequency domain at R_L for the second case model (figure 7.14(b)) at two different values of V_{bias}. Figure 7.15(a) shows the output voltage at R_L when V_{bias} equal to 0.8V and its frequency domain spectral shown in figure 7.16(b). While figure 7.16(c) shows the output voltage at R_L when V_{bias} equal to 1.1V and its frequency domain spectral shown in figure 7.16(d). From the frequency spectral we noticed that there are two main frequencies 7.1 and 14.4 GHz appeared when V_{bias} equal to 0.8 and only 14.4 GHz appeared at 1.1 V_{bias}.

Figure 7.17 shows the simulation output voltage in time and frequency domain at R_L for the third case model (figure 7.14(d)) at two different values of V_{bias}. Figure 7.17(a) shows the output voltage at R_L when V_{bias} equal to 0.9V and its frequency domain spectral shown in figure 7.17(b). While figure 7.17(c) shows the output voltage at R_L when V_{bias} equal to 1.1V and its frequency domain spectral is shown in figure 7.16(d). From the frequency spectral we noticed that there are one main frequency 14.4 GHz appeared when V_{bias} equal to 0.9 or 1.1 V.

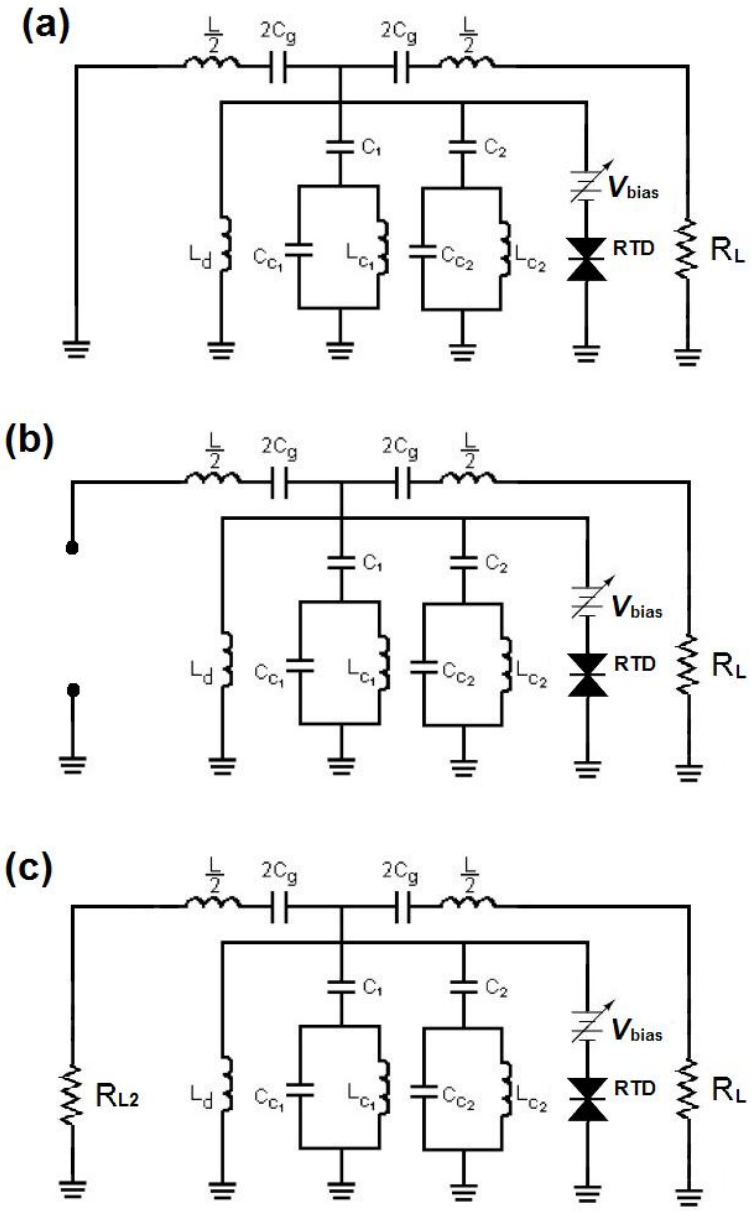

Figure 7.14: Equivalent circuit model of the unit cell (figure 6.4) with RTD shunt with grounded stubs. (a) short circuit at the beginning of the cell between ground and patch, while at the end of the cell is 50 Ω load resistance between ground and patch. (b) open circuit at the beginning of the cell between ground and patch, while at the end of the cell is 50 Ω load resistance between ground and patch. (c) two 50 Ω load resistances between ground and patch at both of beginning and end of cell.

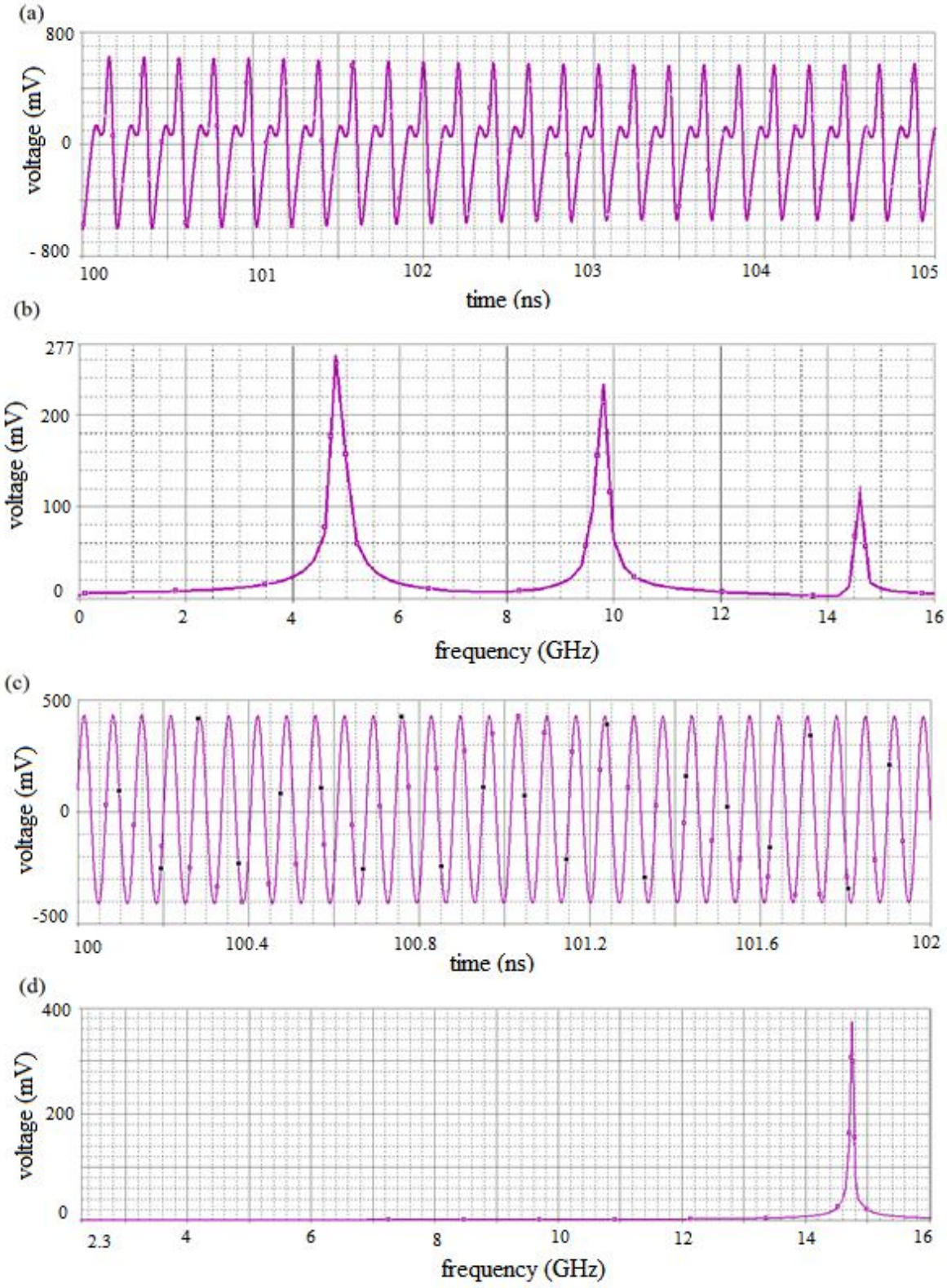

Figure 7.15: the simulation output voltage in time and frequency domain at R_L for the first case model (figure 7.14(a)) at two different values of $V_{bias.}$ (a, b) when V_{bias} equal to 0.7V (c, d) when V_{bias} equal to 1.1V.

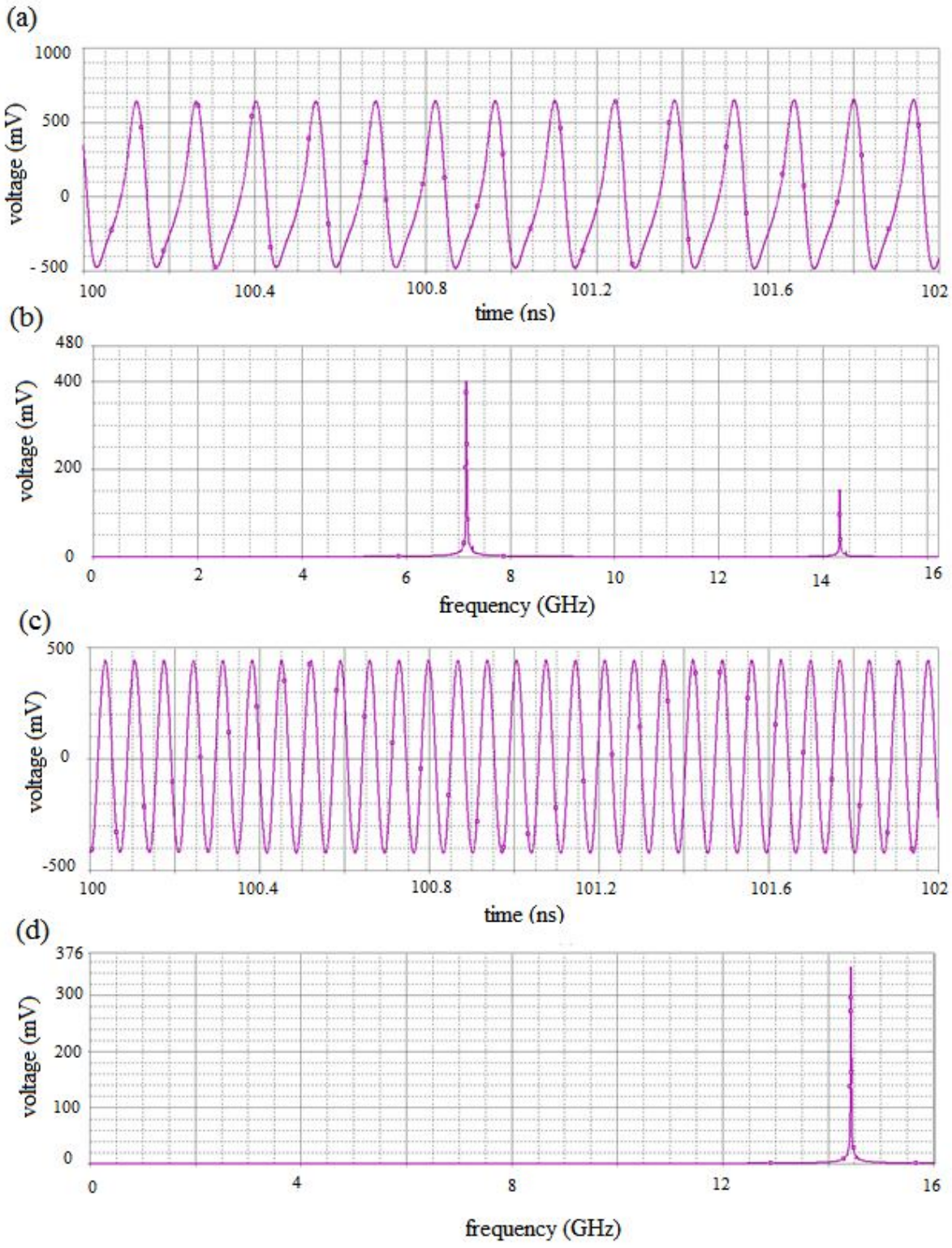

Figure 7.16: The simulation output voltage in time and frequency domain at R_L for the second case model (figure 7.14(b)) at two different values of $V_{bias.}$ (a, b) when V_{bias} equal to 0.9V (c, d) when V_{bias} equal to 1.1V.

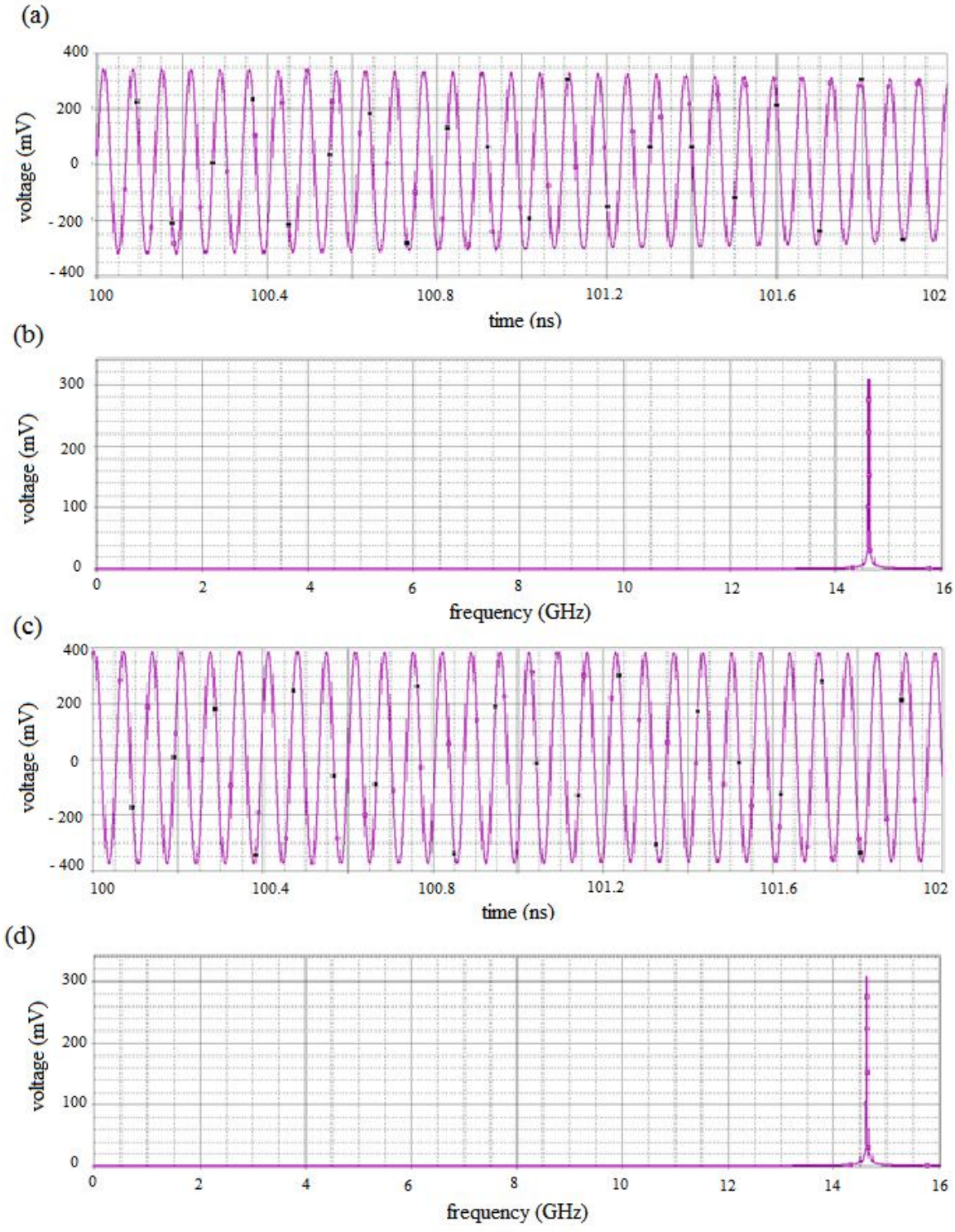

Figure 7.17: The simulation output voltage in time and frequency domain at R_L for the third case model (figure 7.14(d)) at two different values of $V_{bias.}$ (a, b) when V_{bias} equal to 0.9V (c, d) when V_{bias} equal to 1.1V.

Table 7.1 shows output voltage at R_L for all three cases model as a form of "cos" function to show the gain of any frequency relative to another. Where the term "Distorted" refers to distorted signal generation at this case. The oscillation frequencies depend on the V_{bias}. From the table 7.1, we notice that there are three main frequencies 4.8, 9.7 and 14.6 GHz at first case and these frequencies alternate according to V_{bias}. There are two main frequencies approximately 7.2 and 14.3 GHz at second case and these frequencies alternate according to V_{bias}. But at the third case, there is one frequency oscillator that do not change for any value of V_{bias}.

To explain why these frequencies appear in all three cases of our study. We simplified the equivalent circuit that shown in 7.14 to a new form as shown in figure 7.18. Where V_{bias} and RTD remained the same as in figure 7.14 while all other components in the circuit are compound in Z_{eq}, where Z_{eq} differs from one case model to the other.

Figure 7.18: Simplified equivalent circuit model of the three cases model in figure 7.14.

Figure 7.19 shows the reactance of Z_{eq} over the frequency in the three cases model where figure 7.19 (a, b, c) related to fist, second and third case respectively. From figure 7.19(a), we notice that there are three resonance frequencies at 5, 10 and 14.8 GHz that is near to three oscillation frequencies that occur in the first model. From figure 7.19(b), we realize that there are two resonance frequencies at 7.9 and 14.4 GHz that is near to two oscillation frequencies that occur in the second model. Figure 7.19(c) present only one resonance frequencies that close to the oscillation frequency of the third case model.

Vbias	First case (mV)	Second case (mV)	Third case (mV)
0.7	293 Cos(2π 4.87G t + Φ_1) + 169 Cos(2π 9.75G t + Φ_2) + 8.7 Cos(2π 14.6G t + Φ_3)	Distorted	Distorted
0.75	389 Cos(2π 4.91G t + Φ_1) + 294 Cos(2π 9.83G t + Φ_2) + 111 Cos(2π 14.7G t + Φ_3)	427 Cos(2π 7.12G t + Φ_1) + 147 Cos(2π 14.2G t + Φ_2)	Distorted
0.8	48 Cos(2π 4.94G t + Φ_1) + 27 Cos(2π 9.89G t + Φ_2) + 9.8 Cos(2π 14.8G t + Φ_3)	462 Cos(2π 7.15G t + Φ_1) + 38 Cos(2π 14.3G t + Φ_2)	Distorted
0.85	280 Cos(2π 4.87G t + Φ_1) + 270 Cos(2π 9.75G t + Φ_2) + 230 Cos(2π 14.6G t + Φ_3)	560 Cos(2π 7.19G t + Φ_1) + 180 Cos(2π 14.3G t + Φ_2)	200 Cos(2π 14.5G t + Φ_1)
0.9	290 Cos(2π 4.89G t + Φ_1) + 275 Cos(2π 9.79G t + Φ_2) + 190 Cos(2π 14.6G t + Φ_3)	600 Cos(2π 7.22G t + Φ_1) + 190 Cos(2π 14.4G t + Φ_2)	240 Cos(2π 14.5G t + Φ_1)
0.95	245 Cos(2π 4.90G t + Φ_1) + 320 Cos(2π 9.82G t + Φ_2) + 252 Cos(2π 14.7G t + Φ_3)	620 Cos(2π 7.25G t + Φ_1) + 160 Cos(2π 14.5G t + Φ_2)	260 Cos(2π 14.6G t + Φ_1)
0.1	280 Cos(2π 4.92G t + Φ_1) + 285 Cos(2π 9.84G t + Φ_2) + 260 Cos(2π 14.7G t + Φ_3)	275 Cos(2π 14.4G t + Φ_1)	300 Cos(2π 14.6G t + Φ_1)
1.05	310 Cos(2π 4.93G t + Φ_1) + 321 Cos(2π 9.87G t + Φ_2) + 181 Cos(2π 14.8G t + Φ_3)	344 Cos(2π 14.4G t + Φ_1)	320 Cos(2π 14.6G t + Φ_1)
1.1	333 Cos(2π 14.7G t + Φ_1)	315 Cos(2π 14.4G t + Φ_1)	250 Cos(2π 14.6G t + Φ_1)
1.15	340 Cos(2π 14.7G t + Φ_1)	280 Cos(2π 14.4G t + Φ_1)	125 Cos(2π 14.6G t + Φ_1)
1.2	270 Cos(2π 14.7G t + Φ_1)	270 Cos(2π 14.4G t + Φ_1)	Distorted

Table 7.1 Output voltage at R_L for all three case models as a form of *Cos* function where G= 10^9 and Φ_1, Φ_2,Φ_3 are the phase angles.

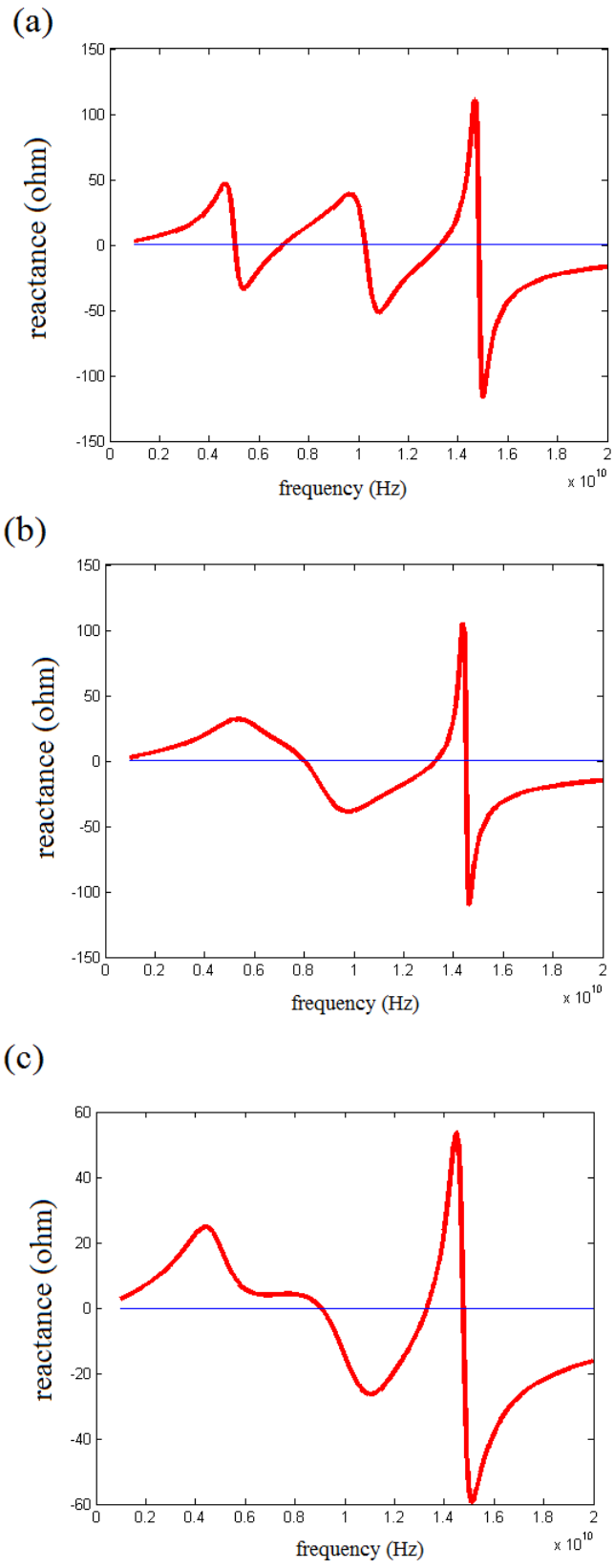

Figure 7.19: Z_{eq} reactance over the frequency in the three cases model. (a, b, c) related to first, second and third case respectively.

8- Conclusion and Future Work

8.1 Conclusion

In this work conclusion, we designed and analyzed a nonlinear CRLH-TL media with Resonant Tunneling Diode (RTD). We designed two applications for CRLH-TL and RTD. The first design is a transmission line capable of filtering and amplifying the signal at very wide bands. The second design is a voltage controlled oscillator. CRLH-TL is based on the hybrid approach, where a microstrip line is loaded with complementary split-rings resonator (CSRR), series gaps, and shunt inductor. The RTD is connected parallel to shunt inductor. In our designs we use a single cell off CSRR, making it simpler and compact.

We design a UWB filter with amplification by added RTD to CRLH-TL hybrid approach. The bandwidth of the filter does not change but additional power is added to the output signal about 50% of the input signal at 1.18 V DC biasing. We used DC source to bias the RTD such that it operates at linear NDR region of the RTD. This filter can amplify the signal at low voltage. Thus, this filter is good in antenna application.

In second application we design VCO by adding RTD to CRLH-TL hybrid approach. Three prototype device examples are designed. The first one is a one cell with short circuit at the beginning of the cell between ground and patch, and 50 Ω load resistance at the end of the cell between ground and patch. The second one is similar to the first prototype but with open circuit at the beginning of the cell instated of short circuit. The third prototype consists of one cell with two 50 Ω load resistances between ground and patch at both the beginning and at the end of the cell. The RTD was biased using a variable DC voltage supply producing voltage oscillator at resistance load. In the first case there are three main frequencies 4.8, 9.7 and 14.6 GHz and these frequencies alternate according to DC biasing, while there are two main frequencies approximately 7.2 and 14.3 GHz at second case and these frequencies alternate according to DC biasing. But at the third case, there is one frequency oscillator equal to 14.6 GHz that do not change for any value of DC biasing from 0.85 to 1.15 V.

8.2 Future Work

- Studying anther type of CRLH-TL like purely resonant-type approach is very important.
- Theoretically, design the CRLH-TL with RTD that has been reached in this thesis by using High Frequency Structure Simulator (HFSS) program.
- RTD with CRLH-TL can be used for other applications ie. to reshape the input signal and ADC.

Bibliography

[1] J. Pendry. "Metamaterials and the Control of Electromagnetic Fields," Conference on Coherence and Quantum Optics, Optical Society of America, New York, 2007.

[2] M. G. Barba. "Resonant-type metamaterial transmission lines and their application to microwave device design, " Doctoral Thesis, Universitat Autònoma de Barcelona, Spain , 2009.

[3] J. Ling. "Resonant Tunneling Diodes: Theory of Operation and Applications," workshop advanced topics in semiconductor device, University of Rochester, Rochester, 2006.

[4] Yan Yan. "silicon-based tunnel diode technology, " Doctoral Thesis, University of Notre Dame , United States, 2008.

[5] M. N. O. sadiku. "Elements of electromagnetics," New York: Oxford university press, 3rd ed, 2001.

[6] T. J. Cui, D. R. Smith and R. Liu. "Metamaterials Theory, Design, and Applications," USA: Southeast University, 2010.

[7] Y. Hao, R. Mittra. "FDTD Modeling of Metamaterials Theory and Applications," artech house, USA, 2009.

[8] Q. Wu, F. Meng, M. Wu, J. Wu and L. Li , "Research on the Negative Permittivity Effect of the Thin Wires Array in Left-Handed Material by Transmission Line Theory," Progress In Electromagnetics Research Symposium, Hangzhou, China, vol. 1, no. 2, pp. 196-200, August 2005.

[9] M. C. Ricci. "superconducting artificial materials with a negative permittivity, a negative permeability, or a negative index of refraction," Doctoral Thesis, University of Maryland, United States, 2007.

[10] J. Zhou , "Study of left-handed materials," Doctoral Thesis, Iowa State University, United States, 2008.

[11] D. R. Smith, W. J. Padilla, D. C. Vier, S. C. Nemat-Nasser and S. Schultz. "Composite medium with simultaneously negative permeability and permittivity", Physical Review Letters, University of California, United States, vol. 84, 2000.

[12] XIN HU. "Some studies on metamaterial transmission lines and their applications," Doctoral Thesis, Sweden University, Sweden, 2009.

[13] J. D. Baena, J. Bonache, F. Martín, R. Marqués, F. Falcone, T. Lopetegi, M. A. G. Laso, J. García, I. Gil, and M. Sorolla, "Equivalent circuit models for split ring resonators and complementary split rings resonators coupled to planar transmission lines," IEEE Trans. Microw. Theory Tech., vol. 53, no. 4, pp. 1415-1461, Apr. 2005.

[14] J. Bonache, M. Gil, O. García-Abad and F. Martín. "Parametric analysis of microstrip lines loaded with complementary split ring resonators," Microwave and Optical Technology Letters, vol. 50, pp. 165-172, 2008.

[15] G. Marta, B. Jordi , G. Joan , M. Jesús and M. Ferran. "Composite right/left-handed metamaterial transmission lines based on complementary split-rings resonators and their applications to very wideband and compact filter design," IEEE transactions on microwave theory and techniques, vol. 55, no. 6, pp. 1296 - 1304, June 2007.

[16] M. Gil, J. Bonache and F. Martin, "Ultra compact band pass filters implemented through complementary spiral resonators (CSRs)," IEEE MTT-S International, Microwave Symposium Digest, vol. 1119, no. 1122, pp. 1119 - 1122, June 2008.

[17] A. Seabaugh, X. Deng, T. Blake, B. Brar, T. Broekaert, R. Lake, F. Morris, and G.Frazier, "Transistors and tunnel diodes for analog/mixed-signal circuits and embedded memory," Int. Electron Dev. Mtg. Technical Digest, pp. 429-432, 1998.

[18] J. Yongsik, C. Sunkyu and Y. Kyounghoon. "Novel Antiphase-Coupled RTD Microwave Oscillator Operating at Extremely Low DC-Power Consumption," IEEE Transactions on Nanotechnology, vol. 9, no. 3, pp. 338 - 341, May 2010.

[19] M. Reddy. "Schottky-collector Resonant Tunnel Diodes for Sub-Millimeter-Wave Applications," Doctoral Thesis, University of California Santa Barbara, United States, 1997.

[20] S. F. Nafea and A. A. S. Dessouki. "An accurate large-signal SPICE model for Resonant Tunneling Diode," IEEE Conference of Microelectronics (ICM), vol. 507, no. 510, pp. 507 - 510, December 2010.

[21] A. Shahhoseini, S. Ghorbanalipour and R. Faez. "Detemining the Thickness of Barriers and Well of Resonance Tunneling Diodes by Specified I-V Characteristic," International Conference on Physics Science and Technology, vol. 110, pp. 5464-5470, 2010.

[22] Zhixin Yan, and M. J. Deen. "New RTD Large Signal DC Model Suitable for PSPICE," IEEE Transactions on Computer-Aided Design of Integrated Circuits and Systems, vol. 14, no. 2, pp. 167 - 172, February 1995.

[23] S. Atsushi, C. Christophe and I. Tatsuo. "Characteristics of the Composite

Right/Left-Handed Transmission Lines," IEEE microwave and wirless components letters, vol. 14, no. 2, pp. 68 - 70, february 2004.

[24] A. B. Kozyrev, D.W. van der Weide. "Nonlinear Wave Propagation Phenomena in Left-Handed Transmission-Line Media," IEEE Transactions on Microwave Theory and Techniques, vol. 53, no. 1, pp. 238 - 245, January 2005.

[25] P. R. Julien and K. S. Anja." Composite Right/Left-Handed Transmission Line Metamaterial Phase Shifters (MPS) in MMIC Technology, " IEEE Transactions on Microwave Theory and Techniques, vol. 54, no. 4, pp. 1582 - 1589, April 2006.

[26] T. J. Slight, B. Romeira, L. Wang, J. M. L. Figueiredo, E. Wasige and C. N. Ironside. "A Liénard Oscillator Resonant Tunnelling Diode-Laser Diode Hybrid Integrated Circuit: Model and Experiment," IEEE journal of quantum electronics, vol. 44, no. 12, pp. 1158 - 1163, December 2008.

[27] H.J. El-Khozondar and I. M. Abo Ireban, "Transmission Lines and Schottky Diode," Master thesis, University of Islamic, Physics Department, Gaza , 2010.

[28] H. J. El-Khozondara, R. J. El-Khozondrab, A. R.S. AL-Farraa and B. Z. Essimbi. "Nonlinear resonant tunneling diode (RTD) circuits for microwave A/D conversion," International Journal for Light and Electron Optics, vol. 124, pp. 6100–6103, 2013.

[29] D. Kuylenstierna, A. Vorobiev, P. Linner and S. Gevorgian. "Composite right/left handed transmission line phase shifter using ferroelectric varactors," IEEE, Microwave and Wireless Components Letters, vol.16, no.4, pp. 167-169, April 2006.

[30] C. Jaewon, K. Hyoungjun, L. Chongmin and S. Chulhun. "Broadband VCO Using Tunable Metamaterial Transmission Line with Varactor-loaded Split-ring Resonator," Progress In Electromagnetics Research Symposium, Hangzhou, China, March 2008.

[31] K. Maezawa, K. Kasahara and M. Mori. "A traveling wave amplifier based on composite right/left handed (CRLH) transmission lines periodically loaded with resonant tunneling diode pairs," IEEE Conference of Indium Phosphide & Related Materials (IPRM), vol. 4, pp. 1- 4, May 2010.

[32] J. García-García, F. Martín, J. D. Baena, and R. Marqués. "On the resonances and polarizabilities of split rings resonators," J. Appl. Phys., vol. 98, Sep. 2005.